Monthly Notices of the ROYAL ASTRONOMICAL SOCIETY

MNRAS **508,** 5786–5801 (2021) https://doi.org/10.1093/mnras/stab2836
Advance Access publication 2021 October 5

NGC 6124: a young open cluster with anomalous- and fast-rotating giant stars

N. Holanda [1]★ N. A. Drake,[2,3] W. J. B. Corradi [2,4] F. A. Ferreira [4] F. Maia [5] L. Magrini [6] J. R. P. da Silva[7] and C. B. Pereira[1]

[1]*Observatório Nacional, Rua General José Cristino 77, CEP 20921-400, São Cristóvão, Rio de Janeiro, RJ, Brazil*
[2]*Laboratório Nacional de Astrofísica/MCTI, Rua Estados Unidos, 154, 37504-364, Itajubá, Brazil*
[3]*Laboratory of Observational Astrophysics, St. Petersburg State University, Universitetski pr. 28, St. Petersburg 198504, Russia*
[4]*Universidade Federal de Minas Gerais, Departamento de Física, Av. Antônio Carlos 6627, 31270-901, Brazil*
[5]*Instituto de Física, Universidade Federal do Rio de Janeiro, 21941-972, Rio de Janeiro, RJ, Brazil*
[6]*INAF – Osservatorio Astrofisico di Arcetri, Largo E. Fermi, 5, I-50125 Firenze, Italy*
[7]*Departamento de Física, Universidade do Estado do Rio Grande do Norte, Rua Prof. Antonio Campos, 59610-090 Mossoró, Brazil*

Accepted 2021 September 24. Received 2021 September 17; in original form 2021 July 2

ABSTRACT

We present the results of a chemical analysis of fast and anomalous rotator giants members of the young open cluster NGC 6124. For this purpose, we carried out abundances of the mixing sensitive species such as Li, C, N, Na, and $^{12}C/^{13}C$ isotopic ratio, as well as other chemical species for a sample of four giants among the seven observed ones. This study is based on standard spectral analysis technique using high-resolution spectroscopic data. We also performed an investigation of the rotational velocity ($v \sin i$) once this sample exhibits abnormal values – giant stars commonly present rotational velocities of few km s^{-1}. In parallel, we have performed a membership study, making use of the third data release from ESA *Gaia* mission. Based on these data, we estimated a distance of $d = 630$ pc and an age of 178 Myr through isochrone fitting. After that procedure, we matched all the information raised and investigated the evolutionary stages and thermohaline mixing model through of spectroscopic $T_{\rm eff}$ and log g and mixing tracers, such as $^{12}C/^{13}C$ and Na, of the studied stars. We derived a low mean metallicity of [Fe/H] $= -0.13 \pm 0.05$ and a modest enhancement of the elements created by the s-process, such as Y, Zr, La, Ce, and Nd, which is in agreement with what has already been reported in the literature for young clusters. The giants analysed have homogeneous abundances, except for lithium abundance [$\log \epsilon(\rm Li)_{\rm NLTE} = 1.08 \pm 0.42$] and this may be associated with a combination of mechanisms that act increasing or decreasing lithium abundances in stellar atmospheres.

Key words: stars: abundances – stars: fundamental parameters – Galaxy: disc – open clusters and associations: individual: NGC 6124.

1 INTRODUCTION

Open clusters are numerous and are distributed throughout the Galactic disc. Based on the assumption that their member stars have the same initial chemical composition, and basically the same distances and ages, they are useful astrophysics laboratories, for a wide variety of topics (e.g. Friel 1995; Lada & Lada 2003; Reddy & Lambert 2019), allowing us to investigate both aspects of stellar physics and evolution and of the global chemical evolution of our Galaxy (e.g. Heiter et al. 2014; Böcek Topcu, Afşar & Sneden 2016; Magrini et al. 2017). In particular, when we study the red giant populations of open clusters by combining information from light elements, which are tracers of the mixing processes (Li, C, N, $^{12}C/^{13}C$, and Na) and heavy elements, we can obtain a privileged perspective on the evolutionary history of cluster stars. In addition, open clusters can host red giants with anomalous (≥ 6 km s^{-1}) and high ($\geq$8–10 km s^{-1}) projected rotational velocity, in which we can investigate the effects of rotation on their abundances, still rarely discussed in the literature, by comparing them with non-rotating member stars.

When stars ascend to the red giant branch (RGB) they experiment a significant expansion, from which we can expect a low surface rotation due to the conservation of angular momentum – the typical rotational velocity for G and K giants is about 2 km s^{-1} (de Medeiros, Melo & Mayor 1996a). Concerning the exceptions, Carlberg et al. (2011) used a sample of 1297 spectral type K giants for a study of rotation and reported the discovery of 28 rapidly rotating giants, with the projected rotation speeds between 10.0 and 86.4 km s^{-1}, which represents 2.2 per cent of all their sample. In this sense, giant stars with high projected rotational velocities are rare and are a challenge for astrophysics.

While studying 761 red giant stars in the solar neighbourhood, Massarotti et al. (2008) reported evidences to support that the first dredge-up may play a role by increasing the rotation of the observable outer layers of giants, hypothesis originally raised by Simon & Drake (1989) for explaining rapidly rotating giants. On other hand, some works argue that coalescence of close binary systems and

★ E-mail: nacizoholanda@on.br

Table 1. Basic information of the observed stars of NGC 6124.

Star	RA (J2000) (h m s)	Dec. (J2000) (d m s)	Type	V^a (mag)	$(B-V)^a$ (mag)	RV^d (km s^{-1})	RV^e (km s^{-1})	RV (km s^{-1})	$v \sin i$ (km s^{-1})	Prob	Remark
#1	16 23 00.975	−40 36 49.349	G6/K0^b	9.111	1.682	− 21.60	− 20.71	−19.97 ± 1.32	17.0	0.99	S
#14	16 24 49.933	−40 45 31.440	K0^b	9.207	1.750	− 21.60	− 20.40	−20.40 ± 0.27	6.8	1.00	S
#29	16 25 28.615	−40 38 55.806	–	9.319	1.729	− 21.17	− 22.22	−16.19 ± 0.65	10.0	0.39	SB1^d
#33	16 25 45.239	−40 40 46.565	M0^c	8.651	1.923	− 20.89	− 42.41	−9.33 ± 2.26	25.5	0.95	SB1^d
#35	16 25 59.799	−40 33 30.614	G5/6^b	9.040	1.678	− 18.97	− 18.53	−17.31 ± 2.18	20.0	0.99	S
#36	16 26 00.429	−40 51 02.541	G2/3^b	9.217	1.840	− 21.42	− 20.82	−21.23 ± 0.22	6.7	0.83	VD^f
#233	16 24 26.392	−40 45 38.433	K0^c	8.893	1.762	− 21.69	− 22.55	−22.68 ± 0.43	6.8	0.99	S

The data were taken from Henden et al. (2015)^a, Houk (1978)^b, Nesterov et al. (1995)^c, Mermilliod et al. (2008)^d, Gaia Collaboration et al. (2018)^e, and Worley & Douglass (1996)^f. Remarks refers to single (S), spectroscopic binary one-lined (SB1), and visual double star (VD).

interactions followed by engulfment of a planet or (sub)companion may also help to explain the origin of rapid rotators (Peterson, Tarbell & Carney 1983; Siess & Livio 1999; Carlberg, Majewski & Arras 2009; Privitera et al. 2016).

Carlberg (2014) found that the red clump stage in their sample of 11 open clusters of intermediate age (0.7–5.01 Gyr) presents a larger incidence of rapid rotator stars, i.e. they confirm that the rotational velocities of intermediate-mass stars have a higher dispersion. Moreover, they present some results for the giant stars in the open cluster Pismis 18 – with the age estimated between 0.7 Gyr (Hatzidimitriou et al. 2019) and 1.2 Gyr (Piatti et al. 1998) – finding a high mean rotational velocity. Thereafter, Delgado Mena et al. (2016) carried out a robust analysis based on high-resolution spectroscopy of a sample composed by 67 red giant stars in 12 different open clusters. Essentially, Delgado Mena et al. determined the evolutionary stage of their sample stars based on their stellar parameters, and discussed the possible scenario of formation of Li-rich stars – the projected rotational velocity has been investigated in the framework of the association between high $v \sin i$ values and engulfment of planets and sub-stellar companions that also may cause overabundance in lithium in the photosphere. Furthermore, the investigation of projected rotational velocity can reveal important aspects concerning the internal stellar structure, magnetic activity, tidal interactions, and consequently the stellar evolution (Carlberg et al. 2011; Deheuvels et al. 2015), topics that are often invoked in the discussion of lithium-rich giant stars.

In this context, NGC 6124 is a young open cluster that has not been studied from the chemical perspective so far. This paper presents the first chemical study of the giant stars in NGC 6124: its low average metallicity relative to the Sun is compatible with the studies of young and intermediate-age open clusters that are in the solar neighbourhood (Biazzo, Randich & Palla 2011; Spina et al. 2014, 2017). Located in Scorpius region (ℓ, b) = (340°.74, +06°.02), its distance was estimated in several works: 435 pc (Koelbloed 1959), 563 pc (Pedreros 1987), 470 pc (Kharchenko et al. 2005), 630 pc (Cantat-Gaudin et al. 2018). At first, it seems to contains eight red giant stars, of which two are spectroscopic binaries (#29 and #33), with orbits determined by Mermilliod, Mayor & Udry (2008), and a visual binary star (#36) with a companion of magnitude $V = 14.2$ reported by Worley & Douglass (1996). Among them, the binary star #33 as pointed by The (1965) and Vergne et al. (2010) is suspected as not being a member of the cluster.

We carried out a study based on seven out of eight giant stars (excluding NGC 6124-#41). The paper is organized as follow. In Section 2, we describe the data and their analysis. After, in Section 3, we present our results for abundances and compare with field stars, mixing models and predictions by galactic chemical evolution models. In addition, we investigate the possible correlations between $v \sin i$, age and Li abundance. Finally, our conclusions are given in Section 4.

2 OBSERVATIONS AND ANALYSIS

2.1 Spectroscopic data

The observations were carried out using the Fiber-fed Extended Range Optical Spectrograph (FEROS; Kaufer et al. 1999) at the 2.2 m Max Planck Gesellschaft/European Southern Observatory (ESO) Telescope in La Silla, Chile, between 2016 March 18 and 20. The FEROS spectra have a resolution $R \equiv \lambda/\delta\lambda \approx 48000$ within the spectral coverage of 3600 – 9200 Å. The exposure time of the high-dispersion ranges from 1200 to 1500 s to achieve a typical signal-to-noise ratio of 150–200. Furthermore, the FEROS Data Reduction System pipeline was used to reduce all spectra. The program stars, like those previously investigated (Sales Silva et al. 2014; da Silveira, Pereira & Drake 2018; Peña Suárez et al. 2018; Holanda, Pereira & Drake 2019; Martinez et al. 2020), were selected based on the radial velocity survey done by Mermilliod et al. (2008).

In the above mentioned recent works, the authors studied the chemical nature and highlighted aspects related to binarity and stellar and chemical evolution of the Galactic disk through the analysis of the open clusters. Here, we present a similar approach for seven giants for which basic information is available in Table 1 – such as coordinates, spectral type given by Houk (1978) and Nesterov et al. (1995), the visual magnitude, the $(B-V)$ colour index and the radial velocities from Mermilliod et al. (2008) and Gaia Collaboration et al. (2018), the projected rotational velocities and probabilities of belonging to NGC 6124 (Prob).

2.2 Membership determination

In order to complement the spectroscopic data, we used the astrometric and photometric data from the Gaia Collaboration et al. (2021) – parallaxes, proper motions, and photometry. Data from ESA *Gaia* Mission were used to carry on a membership analysis and to estimate the size, distance moduli, reddening, age, and turn-off mass of NGC 6124. We estimated the size of the cluster by building a radial density profile; a similar procedure performed in Angelo et al. (2019) and restricted the parameters space of our data to the one represented by the cluster stars distribution by applying a box shaped filter in proper motions and parallax, centred by the values $(\mu_\alpha^*, \mu_\delta, \pi) = (-0.40\ \mathrm{mas\ yr^{-1}}, -2.16\ \mathrm{mas\ yr^{-1}}, 1.55\ \mathrm{mas})$, and with box sizes of 4.0 mas yr^{-1} in proper motion and 1.0 mas in parallax.

The membership likelihoods were derived by applying a routine described in Ferreira et al. (2020); this routine statistically evaluates

the overdensity of stars centred at the cluster's coordinates and restricted by its limiting radii in comparison to those in a nearby Galactic field in the 3D astrometric space. The list of cluster members was built by keeping stars with membership probabilities higher than 80 per cent and present a total of 1065 stars belonging to NGC 6124. Furthermore, we performed isochrone fittings on the colour magnitude diagram of this decontaminated cluster sample to determine age, distance moduli and reddening by employing PARSEC-COLIBRI models (Marigo et al. 2017). The procedure was made by visually inspecting the match between the model and the cluster stars loci centred in specific evolutionary regions (main sequence, the turn-off, and red clump). We then converted $E(G_{BP} - G_{RP})$ to $E(B - V)$ by adopting a reddening law (Cardelli, Clayton & Mathis 1989; O'Donnell 1994); this last one correspond to $E(B - V) = 0.72 \pm 0.04$, which is in good agreement with $E(B - V) = 0.80$ found by Pedreros (1987) and Vergne et al. (2010). After all, this procedure confirms the best-fit around of log $t = 8.25$ (or 178 Myr) isochrone. The dispersion of stars in the main-sequence and turn-off stage in our adjustment can be a contribution of high rotation, binarity and differential reddening; this cluster is projected near the edge of a dark cloud which obscures some of its stars, and explains its differential reddening [$\Delta E(B - V) = 0.20$] verified by Pedreros and later endorsed by Vergne et al. (2010). Some these aspects are widely discussed for massive and intermediate clusters in Sun et al. (2019a), Sun et al. (2019b) and are not addressed in the present work. Note, features such as differential reddening were not considered for the performing best fit, although we have used two additional isochrones in Fig. 1 to represent our uncertainties in the age. The basic parameters of NGC 6124 are given in Table 2.

Fig. 1 presents a complete overview about our final results: the vector point diagram for brightest stars around the centre of NGC 6124 (top left), magnitude versus parallax (bottom left), colour–magnitude diagram with an isochrone fitting (top right), and the spatial distribution of stars in the cluster region (bottom right). The giant stars analysed in this work are represented by red circles (single stars or members in wide binaries), while green circles represent spectroscopic binaries. The probabilities of belonging to NGC 6124 as derived from our astrometric analysis for these giant stars are 1.0 (#14), 0.99 (#1, #35, #233), 0.95 (#33), 0.83 (#36), and 0.39 (#29), respectively.

2.2.1 Are NGC 6124-33 and NGC 6124-29 members of the cluster?

Based on the results obtained by polarimetic analysis, Vergne et al. (2010) reinforced the hypothesis raised by The (1965) that NGC 6124-33 could not be a cluster member. Classified as a M0III-type star by Nesterov et al. (1995), this star until then had been considered as a background star. However, we did not find any evidence based on astrometric data – proper motion and parallax – from *Gaia* data. Fig. 1 shows that NGC 6124-33 has similar values to those of the stars of the cluster. As far as the radial velocity is concerned, NGC 6124-33 exhibits a radial velocity value that is discrepant from the other giants (Table 1), but it is possible that this effect could be due to binarity as indicated by Mermilliod et al. (2008).

NGC 6124-29 was classified by Mermilliod et al. (2008) as spectroscopic binary and presents variation in radial velocity of the order of $\approx 3\,\mathrm{km\,s^{-1}}$. In our chemical analysis, this spectroscopic binary shows a chemistry similar to the other three giants analysed here (Fig. 8). However, unlike the other stars in our sample, NGC 6124-29 has a low astrometric probability of belonging to the cluster. Fig. 1 shows astrometric data obtained from *Gaia* DR3 and NGC 6124-29 is an outlier in the cluster parallax distribution. Comparing with the astrometric data from the *Gaia* DR2, we observe variations of $\Delta\mu_\alpha^* = -0.97$, $\Delta\mu_\delta = +0.09$, and $\Delta\pi = -0.34$ which may be due to effects of its binarity.

Beyond the sample of 7 spectroscopically observed giant stars – and NGC 6124-41 –, two other giant stars seems to share the same parameters space presented by the cluster. The star *Gaia* DR2 5993925589460035712 (RA = 16 22 34.882; Dec. = −40 12 37.366), a highly probable member according to our membership analysis ($P = 99$ per cent), with astrometric parameters compatible to the cluster ones by 1σ in π and μ_α^* and 2σ in μ_δ. This star seems to be a red giant brighter than the brightest stars expected for a cluster of this age (according to our isochrone fitting).

The star *Gaia* DR2 5992807351770974976 (RA = 16 29 09.699; Dec. = −41 37 29.455), which according to our analysis is a field star located at a distance of 72.6 arcmin from the cluster centre (farther than the cluster limiting radii), could be a subgiant star according to its position in the colour–magnitude diagram. The star's astrometric parameters are compatible to the cluster space by $1\,\sigma$ in μ_δ, $2\,\sigma$ in π and $3\,\sigma$ in μ_α^*. This object is classified as 'Probable Member' by Baumgardt, Dettbarn & Wielen (2000) in their study with astrometric data taken from *Hipparcos* Catalogue.

The sample of 10 post-main-sequence stars (7 spectroscopically studied and the 2 stars mentioned above) is presented in the cluster memberlist from Cantat-Gaudin et al. (2018). The authors use *Gaia* DR2 data and their analysis assigns membership probabilities higher than 70 per cent for this sample of stars, except to NGC 6124-29 ($P = 20$ per cent). It suggests that all of the mentioned stars are possible cluster members.

2.3 Atmospheric parameters

Following the recent results of Baratella et al. (2020), we adopted neutral and ionized titanium and iron lines to derive the stellar parameters. Baratella et al. (2020), indeed, found that in stars with high chromospheric activity, the microturbulent velocity derived from iron lines might be overestimated, implying an underestimation of the metallicity. Since our targets are giant stars with notable $v \sin i$ values, which may results in chromospheric activity and can be related to enrichment in lithium (e.g. Fekel & Balachandran 1993) and Drake et al. (2002), we adopted the method of Baratella et al. (2020).

The atmospheric parameters of the giants #14, #29, #36, and #233 in NGC 6124 were obtained interpolating the grid of local thermodynaminal equilibrium (LTE) plane-parallel atmospheric models of Kurucz (1993) and the radiative transfer code MOOG (2013 version; Sneden 1973). The respective log gf values and excitation potentials (χ) were taken from Lawler et al. (2013), Wood et al. (2013), and Lambert et al. (1996, Table A1). Essentially, this list is formed by lines carefully chosen for the purpose to eliminate blended lines and reduce potential contamination by molecular bands that are formed naturally in cool giant atmospheres. In conjunction with this, we used IRAF to measure the equivalent widths (EW) using the Gaussian fit with the task SPLOT. After that, the spectral analysis code MOOG was used for the determination of the stellar atmospheric parameters and abundances of the interest chemical species.

The atmospheric parameters were determined in a way similar to the one adopted by Baratella et al. (2020) according to the following three steps: (i) the effective temperature ($T_{\rm eff}$) was obtained by

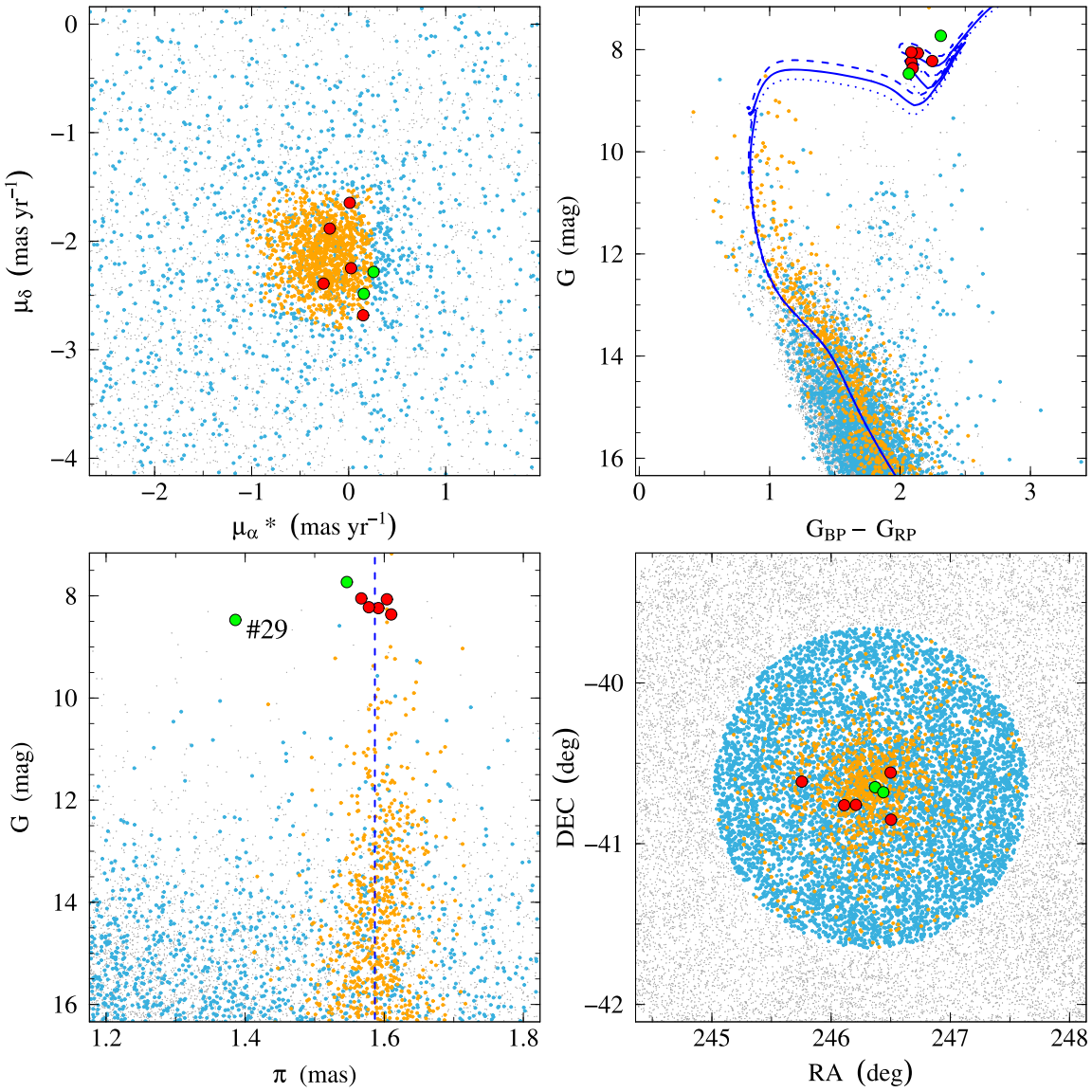

Figure 1. Proper motion distribution for bright stars around of the centre of NGC 6124 (top left), where the blue and orange points represent stars with probability to belonging to cluster of $0 \leq P < 0.8$ and $P \geq 0.8$, respectively. Small grey points represent field stars. Magnitude versus parallax (bottom left), where blue dashed line represents the mean parallax for this open cluster. Colour–magnitude diagram (top right) is shown with an isochrone fitting (Marigo et al. 2017) for stars with proper motions and parallaxes characteristics of the cluster and NGC 6124-29 giant (log t = 8.20, 8.25, 8.30). Bottom right represents the plane of distribution of stars around the cluster, with a limit radius of 3587 ± 115 arcsec. The stars analysed in this work are represented by red and green (spectroscopic binaries) points. Data were taken from Gaia Collaboration et al. (2021).

imposing the condition that the abundance of Ti I and Fe I lines[1] does not depend on the lower-level excitation potential; (ii) the microturbulence velocity (ξ) was found requiring that the abundance of Ti I lines does not depend on the reduced equivalent width (EW/λ); (iii) also, the surface gravity (log g) was found from the ionization equilibrium. Steps (i) and (ii) can be verified through the slopes of linear adjustment of both cases with values close to zero (Fig. 2). In this research, we adopt an absolute limit of 0.008 for each slope coefficients and applied a criteria of $2\,\sigma$ clipping rejection for these titanium and iron lines. We checked the differences between the standard method (only iron) and the Baratella et al. (2020)'s one, finding $\Delta T_{\rm eff} = +103$ K, $\Delta \log g = +0.08$ dex, $\Delta\xi = +0.17$ km s^{-1}, Δ[Fe/H] $= -0.07$ dex. The fundamental parameters, obtained by this method, are given in Table 3.

The uncertainties in the temperature and microturbulent velocity were estimated from the uncertainties in the slopes of relationships described before. The standard deviation in the abundance of Ti I and Fe I were used to provide the uncertainty in the log g parameter. In general, we have found typical uncertainties in the temperature, microturbulent velocity, and surface gravity of $\sigma(T_{\rm eff}) = \pm 90$ K, $\sigma(\xi) = \pm 0.2$ km s^{-1}, and $\sigma(\log g) = \pm 0.1$, respectively.

Furthermore, it was not possible to apply the described method to all spectra obtained in our observational mission, since three stars (#1, #33, and #35) have very high $v \sin i$ (Table 1). Fig. 3 shows

[1]All abundances in the notation: [X/H] = $\log(N_X/N_H)_\star - \log(N_X/N_H)_\odot$

Table 2. NGC 6124 cluster parameters.

Right ascension (deg)	246.333	This work
Declination (deg)	−40.653	This work
log t (Gyr)	8.25 ± 0.05	This work
log t (Gyr)	8.147	Dias et al. (2002)
$M_{\rm turn\text{-}off}$ ($M_\odot$)	3.95 ± 0.18	This work
d (pc)	630 ± 24	This work
d (pc)	563	Pedreros (1987)
d (pc)	630.5	Cantat-Gaudin et al. (2018)
π (mas)	1.586 ± 0.062	This work
π (mas)	1.557	Cantat-Gaudin et al. (2018)
$R_{\rm GC}$ (kpc)	7.41 ± 0.02	This work
$E(B-V)$ (mag)	0.72 ± 0.04	This work
$E(B-V)$ (mag)	0.80	Pedreros (1987)
$V-M_V$ (mag)	8.90 ± 0.10	This work
pmRA (mas yr^{-1})	−0.264 ± 0.269	This work
pmDEC (mas yr^{-1})	−2.129 ± 0.275	This work

absorption lines around the Hα line for our sample of stars. That said, we have used the atmosphere models based on iron abundance of −0.13 (the mean of four giants with equivalent width measured), microturbulence velocity of 2.0 km s^{-1}, and photometric log g and $T_{\rm eff}$ for these stars. We adopted the polynomials found by González Hernández & Bonifacio (2009) for fitting $(B-V)$ colour as function of $T_{\rm eff}$ and for photometric gravity we applied the well-known expression:

$$\log g_\star = \log\left(\frac{M_{\rm turn-off}}{M_\odot}\right) + 0.4\,(V - A_V + BC_V) + 4\,\log T_{\rm eff} - 2\,\log d\,({\rm kpc}) - 16.5,$$

where V, A_V, and $BC_{\rm V}$ are, respectively, the visual magnitude, interstellar absorption in V band and bolometric correction. The surface gravity, turn-off mass, and temperature of the star are, respectively, log $g_\star$, $M_{\rm turn\text{-}off}$ and $T_{\rm eff}$ and d is the heliocentric distance of the open cluster given in kpc. The Solar values used in this expression are $M_{\rm bol} = 4.75$, log $g = 4.44$, and $T_{\rm eff} = 5777$ K, as well the bolometric corrections were calculated using the relation given in Alonso, Arribas & Martínez-Roger (1999). The corresponding mean differences between the spectroscopic and photometric temperature is +182 ± 141 K and in log of gravity is −0.02 ± 0.12 cm s^{-2}. Yet, it is possible that our photometric $T_{\rm eff}$ values based on $B-V$ colour contain uncertainty due to differential reddening, especially for the stars #36 and #233.

2.4 Abundance determination

As said before, we have used both equivalent widths and spectrum synthesis for the abundance analysis. We measured the equivalent widths of the elements Na, Mg, Al, Si, Ca, Ti, Cr, Ni, Y, Zr, La, Ce, Nd, and Sm in order to obtain their abundances. The line list used is given in Table A2, with their respective excitation potentials (χ) and log gf (Sales Silva et al. 2014 and references therein). All lines were inspected in order to avoid the blending between lines, hence the final line list differs slightly from star to star.

The abundances of lithium, carbon and nitrogen, the ^{12}C/^{13}C isotopic ratio and europium were determined in the same way as in Holanda et al. (2019). Unfortunately, we could not obtain the oxygen abundance based on the forbidden line at λ 6300 Å because of the contamination with telluric O_2 lines. Also, the line [O I] at 6363 Å is unsuitable because it is weak and contaminated by a CN line. Knowing this, we assumed [O/H] = 0.0 to estimate the carbon and nitrogen abundances, since occurs an interdependence between them. However, variation in oxygen abundance cause small changes in carbon and nitrogen abundances: for the star NGC 6124-36, when we change the oxygen abundance by +0.20, we verify a variation +0.03 and +0.08 in carbon and nitrogen abundances, respectively.

The carbon abundance was determined using the C_2 (0,1) band head of the Swan system $A^3\Pi_g - X^3\Pi_u$ at 5 635 Å – where the wavelengths were taken from Phillips & Davis (1968), the electron oscillator strength from Lambert (1978), and the C_2 dissociation energy from Huber & Herzberg (1979), while the nitrogen abundance and ^{12}C/^{13}C were obtained by adjusting the theoretical and observed spectra for the ^{12}CN lines of the (2,0) band of the CN red system

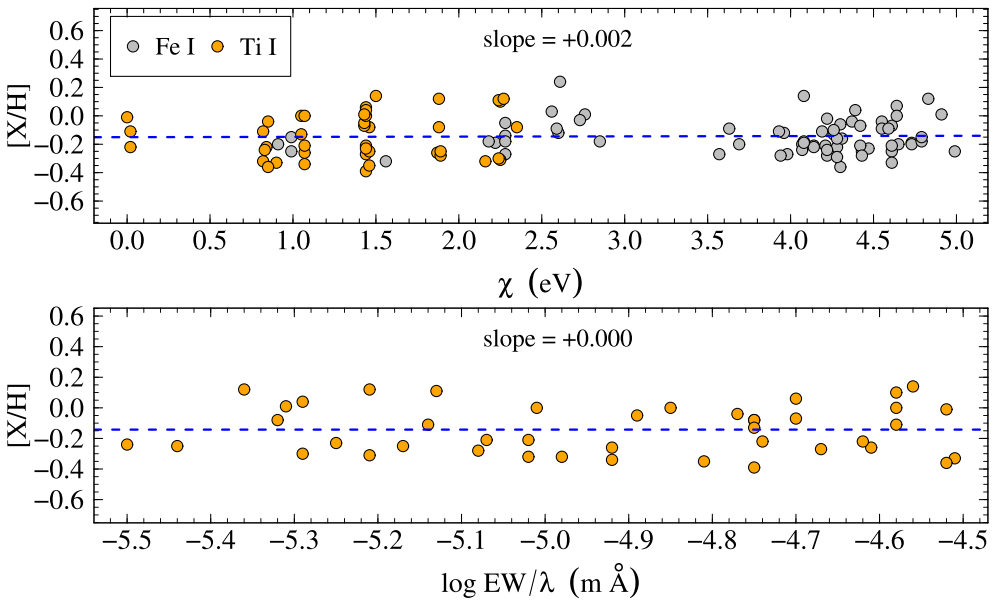

Figure 2. Fe I and Ti I abundances versus excitation potential (χ) and reduced equivalent width (log EW/λ). The blue dashed lines in both panels are the linear regression, and individual slope are expressed on each panel.

Table 3. Determined spectroscopic atmospheric parameters for the giant stars of NGC 6124.

Star	$T_{\rm eff}$ (K)	log g	ϵ (km s^{-1})	[Fe I/H] $\pm\sigma$	[Fe II/H] $\pm\sigma$	$T_{\rm eff}^{(B-V)}$ (K)	log g^{phot}
#1	–	–	–	–	–	4712	1.82
#14	4660	1.70	1.78	-0.11 ± 0.14 (72)	-0.16 ± 0.11 (13)	4592	1.79
#29	4680	2.00	1.88	-0.14 ± 0.12 (62)	-0.14 ± 0.14 (9)	4627	1.85
#33	–	–	–	–	–	4336	1.39
#35	–	–	–	–	–	4719	1.79
#36	4770	1.55	2.18	-0.15 ± 0.12 (68)	-0.15 ± 0.12 (11)	4450	1.70
#233	4860	1.60	2.00	-0.10 ± 0.13 (75)	-0.13 ± 0.06 (10)	4572	1.65

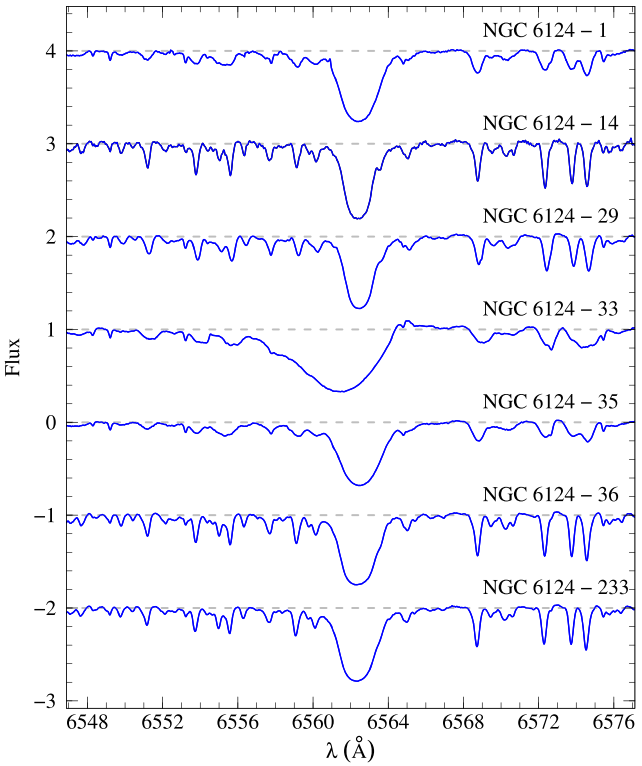

Figure 3. Observed spectra in the region H α of the giants of NGC 6124.

$A^2\Pi - X^2\Sigma$ in the 8004 Å region – the wavelengths for ^{12}CN and ^{13}CN were taken from Davis & Phillips (1963) and Wyller (1966), the oscillator strength from Sneden & Lambert (1982), and the CN dissociation energy from Sneden & Lambert (1982) and Bauschlicher, Langhoff & Taylor (1988). Drake & Pereira (2008) provide details about the atomic and molecular parameters used in the construction of the input files for the spectral synthesis.

The lithium abundance was determined by spectral synthesis of the resonance λ 6708 Å line. We took the wavelengths and oscillator strengths from Smith, Lambert & Nissen 1998 and Hobbs, Thorburn & Rebull (1999) and assumed an isotopic ratio ^{6}Li/^{7}Li = 0.0. After finding ^{7}Li abundance under LTE conditions, we performed corrections for NLTE effects based on the Lind, Asplund & Barklem (2009) grids. Both results are shown in Table 4, where we can note that there was an increase in abundance for this element if we consider the NLTE effects in λ 6708 Å line. In addition to lithium, we also consider corrections for NLTE effects for the sodium lines analyzed in this work – Na 4752λ, 5149λ, 6154λ, and 6161λ lines – according to the grids computed by Lind et al. (2011). For corrections related to sodium abundance, there was a decrease in abundance in all the lines measured and our results are shown in Table 5. Further, the europium abundances were obtained via synthetic spectra at λ 6645.13 Å. We used the atomic parameters by Lawler et al. (2001) and the hyperfine splitting from Mucciarelli et al. (2008).

As an example of the spectral synthesis method used in the work, Fig. 4 shows a comparison between the theoretical spectrum and the observed spectrum (grey crosses). Our best fits are represented by the red solid line.

All abundances, those obtained by measuring the equivalent widths and those obtained with the spectral synthesis technique, were normalized using the solar abundances of Asplund et al. (2009) and are given in Tables 4 and 5. The equivalent widths measured for each species are shown in Table A2.

3 DISCUSSION

3.1 Rotation velocities

Stellar rotation is inferred through the projected rotational velocity, v sin i, and is a powerful characteristic that relates to many aspects for stellar evolution theory and understanding of internal structure. To estimate the contributions of rotational velocity in the chemical profile of the giants analyzed here, we determined the v sin i by using spectral synthesis of the Fe I 6151.6 Å line. We fixed macroturbulent velocity at 3.0 km s^{-1} – as in Fekel (1997) for G and K giants – and considered the instrumental broadening of the FEROS spectral resolution (FWHM ≈ 0.13), while v sin i was obtained using an iterative procedure until we find smallest deviation between the synthetic and observed spectra. Fig. 5 shows two examples of this procedure, where the best fit to the observed spectra is represented by solid red lines.

To compare our results with relevant literature studies, we show in Fig. 6 the temperature distribution as a function of the projected rotational velocity obtained from Carlberg et al. (2011) for their sample of giant stars and for open cluster giant stars studied in Santrich, Pereira & Drake (2013), Sales Silva et al. (2014), da Silveira et al. (2018), Holanda et al. (2019), and Martinez et al. (2020). In the plot, we highlight the binary stars (green circles), since binarity can affect the stellar angular momentum. This comparison reveals the atypical nature from the rotational perspective for giants belonging to NGC 6124, where the slower rotating giant presents v sin i = 6.7 km s^{-1}. In addition, binaries as #29 and #33 are subject to tidal interactions typical of close binary systems and, therefore, permit us associate these abnormal $v\,sin\,i$ values to their binary nature. Still, the star #33 shows an asymmetric Hα profile (Fig. 3), which is associated to a high activity that also is common in close binary systems. The other objects analysed here are single stars or components in wide systems and the mechanism behind their abnormal rotation is supposed a different one. The masses of the giants analysed in this work are significantly high compared to the masses subject to the Kraft break (Kraft 1966, 1970), so these stars are little affected during the

Table 4. Light element abundances and $^{12}C/^{13}C$ ratio.

Star	log ϵ(Li) LTE	log ϵ(Li) NLTE	[C/Fe]	[N/Fe]	$^{12}C/^{13}C$
#14	+0.15	+0.47	−0.05	+0.48	22
#29	+1.07	+1.39	−0.03	+0.56	14
#36	+0.91	+1.11	−0.10	+0.50	20
#233	+1.15	+1.34	−0.15	+0.56	23
Mean	+0.82 ± 0.46	+1.08 ± 0.42	−0.08 ± 0.05	+0.53 ± 0.04	20 ± 4

Table 5. Abundance ratios [X/Fe] and the standard deviations for the targets in NGC 6124. 'iron-peak', α and *s* refers to the average for iron-peak (Cr, Ni), α-elements (Si, Ca, Ti, Mg) and *s*-elements (Y, Zr, La, Ce, Nd) abundances, respectively.

[X/Fe]	#14	#29	#36	#233	⟨[X/Fe]⟩
Na I	+0.16 (2)	+0.21 (2)	+0.30 (2)	+0.25 (3)	+0.23 ± 0.06
Na I_{NLTE}	+0.09 (2)	+0.15 (2)	+0.22 (2)	+0.20 (3)	+0.17 ± 0.06
Mg I	+0.11 (5)	+0.14 (3)	+0.12 (2)	+0.14 (4)	+0.13 ± 0.02
Al I	+0.05 (5)	+0.05 (4)	+0.03 (3)	+0.04 (4)	+0.04 ± 0.01
Si I	+0.14 (8)	+0.17 (5)	+0.17 (6)	+0.17 (8)	+ 0.16 ± 0.02
Ca I	+0.00 (10)	+0.00 (6)	+0.00 (6)	+0.10 (10)	+0.03 ± 0.05
Ti I	− 0.01 (45)	+0.03 (36)	− 0.04 (42)	− 0.03 (43)	− 0.01 ± 0.03
Ti II	+0.03 (5)	+0.05 (5)	− 0.03 (5)	− 0.02 (6)	+0.01 ± 0.04
Cr I	+0.04 (16)	+0.04 (11)	− 0.07 (16)	− 0.05 (13)	− 0.01 ± 0.06
Ni I	+0.05 (14)	+0.00 (13)	− 0.03 (17)	− 0.01 (18)	+0.00 ± 0.03
Y II	− 0.02 (2)	+0.05 (2)	+0.02 (3)	+0.12 (4)	+0.04 ± 0.06
Zr I	− 0.01 (4)	+0.00 (5)	− 0.04 (6)	+0.09 (5)	+0.01 ± 0.06
La II	+0.19 (4)	+0.25 (2)	+0.14 (3)	+0.12 (3)	+0.18 ± 0.06
Ce II	+0.10 (7)	+0.11 (5)	+0.06 (5)	+0.20 (7)	+0.10 ± 0.03
Nd II	+0.17 (8)	+0.17 (5)	+0.09 (10)	+0.18 (9)	+ 0.15 ± 0.04
Sm II	+0.20 (3)	+0.18 (6)	+0.09 (7)	+0.08 (10)	+ 0.14 ± 0.06
Eu II	+0.11 (1)	+0.17 (1)	+0.09 (1)	+0.09 (1)	+ 0.12 ± 0.04
iron-peak	+0.05	+0.02	− 0.05	− 0.03	+0.00 ± 0.05
α	+0.06	+0.09	+0.06	+0.09	+0.08 ± 0.02
s	+0.09	+0.12	+0.05	+0.14	+0.10 ± 0.04

main sequence phase and retain their angular momentum of birth or suddenly acquired during an angular momentum dredge-up, stellar merge or engulfment of a planet or brown dwarf at the ascent to RGB.

Looking at the population of giants taken from intermediate and young open clusters, Fig. 7 shows the diagram with the mean $v \sin i$ as a function of the age of the clusters with data taken from Carlberg (2014), Delgado Mena et al. (2016) and Santrich et al. (2013), da Silveira et al. (2018), and Holanda et al. (2019): for this comparison, we have excluded all-known binaries and non-confirmed member stars by Mermilliod et al. (2008). Furthermore, there are clusters in common between our previous works and Delgado Mena et al.'s sample (NGC 2360, NGC 2539, NGC 3114, NGC 3680, and NGC 5822), so we have choose the results with more valid targets even though both studies present very similar $< v \sin i >$ values, $| \Delta_{<v \sin i>} | \leq 1.53\,\mathrm{km\,s^{-1}}$, for the same open clusters. Only in clusters NGC 3114 and NGC 2539 present stars in common between the previous studies of our group and the large sample from Delgado Mena et al. (2016), and there is good agreement between their results despite having been obtained via different methodologies. The average differences are 1.20 ± 0.25 and 0.72 ± 0.43 for clusters NGC 3114 and NGC 2539, respectively.

We observe that in fact older clusters (with giants of relative lower mass) have lower $< v \sin i >$ while in younger clusters $< v \sin i >$ increases, although we have only five clusters with age > 1.5 Gyr. Yet, excluding the spectroscopy binaries (#29 and #33), we obtained a mean of 11.46 km s^{-1} (red circle in Fig. 7), which is still considered a high value compared with other cluster with similar age.

Above all, Fig. 7 confirms Carlberg's observations that noted a large dispersion and incidence of fast rotators in stars with relative 'high' mass (the sample comprises only objects with 1.3–2.2 $M_\odot$). Nevertheless, it is important to note that in young clusters such as NGC 6124 the number of giant stars is relatively small and, moreover, spectroscopic sampling for most studies is incomplete for the population of red giant stars. Another critical point is the evolutionary status for each star in an analysis like this; many stars have an position ambiguous in the colour–magnitude diagram if we consider uncertainties sources like differential reddening and rotation and error attributed to atmospheric parameters in the case of the L–$T_{\rm eff}$ diagram.

3.2 Abundances

In this section, we present the results for abundances for C (C_2), N (CN), Li I, Na I, Mg I, Al I, Si I, Ca I, Ti I, Ti II, Cr I, Ni I, Y II, Zr I, La II, Ce II, Nd II, Sm II, and Eu II and $^{12}C/^{13}C$ isotopic ratio. For a better discussion and comparison, we use three robust chemical studies from the literature that investigated giant and dwarf stars in the solar neighbourhood: Luck & Heiter (2007) that carried out stellar parameters and abundance data for a sample of 298 nearby giants; Mishenina et al. (2006) that provided the fundamental parameters

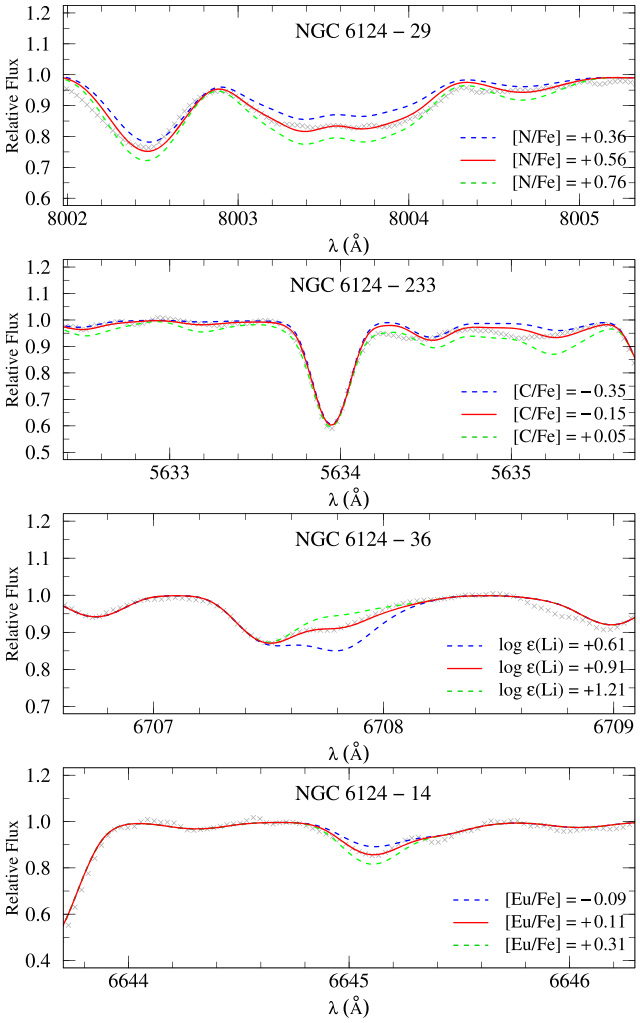

Figure 4. Observed (grey crosses) and the synthetic best-fitting (red line) spectra.

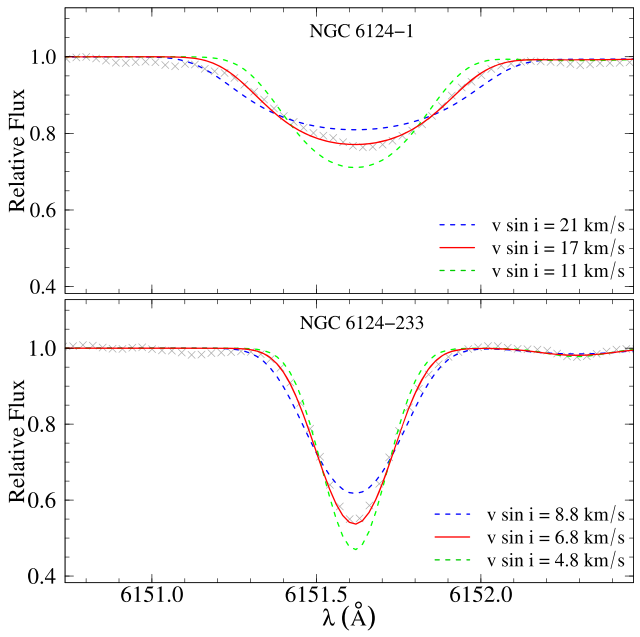

Figure 5. Examples of the projected rotational velocity v sin i determination for the stars NGC 6124-1 and NGC 6124-233, in the region of the Fe I line at 6151.6 Å. Synthetic spectra (colourful lines) for three different values of v sin i and observed spectra (grey crosses) are shown.

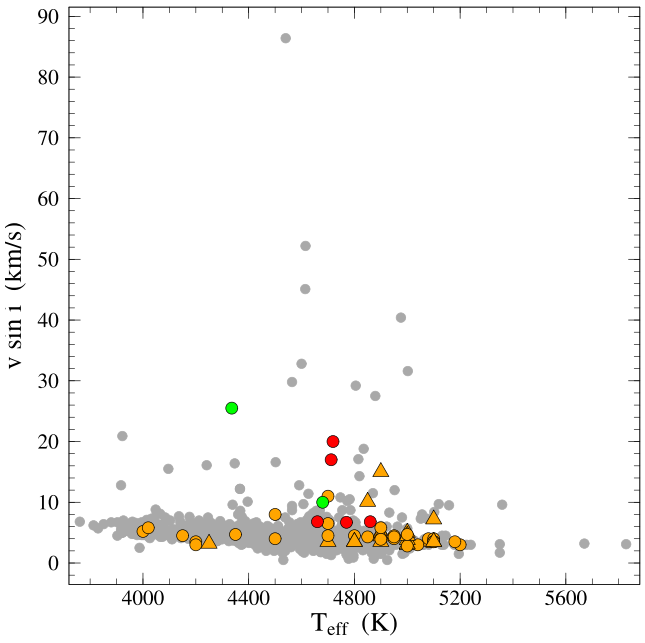

Figure 6. Mean projected rotational velocities, v sin i, for giant stars as a function of temperature. Obtained results for giants in NGC 6124 compared to the samples studied by Carlberg et al. (2011) (grey) and our previous works (Santrich et al. 2013; Peña Suárez et al. 2018; da Silveira et al. 2018; Holanda et al. 2019; Martinez et al. 2020), which orange circles represent single stars and orange triangles represent spectroscopic binaries. The stars analysed in this work are shown as red circles (single or members in wide binaries) and green circles (spectroscopic binaries).

and abundances for a sample composed by 177 of the local clump giants; and Battistini & Bensby (2016) that obtained abundances for heavy elements ($Z > 26.0$) for a sample of 593 F and G dwarf stars. Fig. 8 shows the [X/Fe] ratio *versus* [Fe/H] abundances with our results and the abundances reported by Luck & Heiter (2007), Mishenina et al. (2006), and Battistini & Bensby (2016). In the following subsections, we will discuss the results for the obtained abundances.

3.2.1 Metallicity

The radial metallicity gradient constitutes one of the most important observational constraints to study the Galactic disc, and its evolution over time can be helpful for studies that aim an understanding of the formation and evolution of the Milky Way (Hou, Prantzos & Boissier 2000; Magrini et al. 2009; Netopil et al. 2016). In this framework, we determined the average metallicity of [Fe/H] = −0.13 for the open cluster NGC 6124 taking into account the four giants with measurable equivalent widths. We derived the Galactocentric distance (R_{GC}) of NGC 6124 considering a R_{GC} of the Sun of 8.0 kpc and adopting the

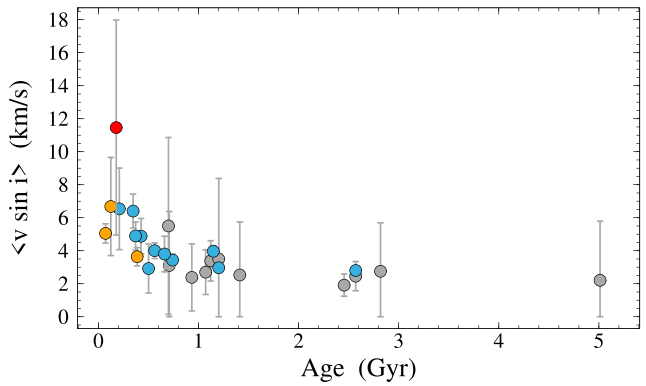

Figure 7. Projected rotational velocities (v sin i) as a function of age. We obtained mean for NGC 6124 cluster – without spectroscopic binaries – and compare to the samples studied by Carlberg (2014) (grey), Delgado Mena et al. (2016) (blue), and open clusters previously studied by our group (orange; Santrich et al. 2013; da Silveira et al. 2018; Holanda et al. 2019).

well-known relation

$$R_{GC}^2 = \mathrm{R}_\odot^2 + (d\ \cos\ b)^2\ -\ 2\,\mathrm{R}_\odot\, d\ \cos\ l\ \cos\ b,$$

where $\mathrm{R}_\odot$ is the Galactocentric distance of the Sun, d is the distance of the cluster to the Sun, and l and b are the Galactic longitude and latitude, respectively.

Fig. 9 shows the radial metallicity gradient of the open cluster sample with red giants homogeneously studied by our group with high-resolution spectroscopy (Santrich et al. 2013; Reddy et al. 2016; da Silveira et al. 2018; Peña Suárez et al. 2018; Holanda et al. 2019; Martinez et al. 2020). The methodology adopted in these selected studies is similar to the one used in this work. We have excluded other samples from the literature to avoid very heterogeneous samples, which might hide nuances of abundances and create differences between chemically similar populations (e.g. Magrini et al. 2014). In Fig. 9, we also included a linear regression for the metallicity trend in the 6–11 kpc interval.

We compared our observations with the semi-analytic multiphase and multizone Galactic chemical evolution (GCE) model of Magrini et al. (2009). Although, there is a good agreement between the model and the observations, the linear fit of the data is slightly flatter than the model. This is likely due to the limited radial interval, and the lack of inner clusters in the sample.

From Fig. 9, we notice that [Fe/H] of NGC 6124 is quite low for its $R_{\rm GC} = 7.41$ kpc. However, at each $R_{\rm GC}$ there is a scatter in the abundances even for the youngest populations. NGC 6124 is not the only young cluster with low metallicity for its location in the Galaxy: NGC 2345 (Alonso-Santiago et al. 2019; Holanda et al. 2019), for example, presents a very atypical metallicity for its Galactocentric distance ([Fe/H] $= -0.33$; Holanda et al. 2019) – NGC 6124 has a low metallicity, but not so significant compared to the of NGC 2345. In a broader context, it is well known in the literature that some young open clusters have slightly sub-solar metallicities (e.g. Biazzo et al. 2011; Spina et al. 2014, 2017; Alonso-Santiago et al. 2018). Their low metallicity is possibly due to the limitation of standard spectral analysis method, which is only based on the inspection of lines of neutral and ionized iron (Baratella et al. 2020).

3.2.2 C, N, and Li elements

We have found homogeneous abundances of carbon and nitrogen in the four analysed giants. In Fig. 8, we show the derived [C/Fe] and [N/Fe] ratios in comparison with the same ratios obtained by Mishenina et al. (2006) and Luck & Heiter (2007) for disc red clump giants and local disc field giants (the results of these references have been normalized to Asplund et al. 2009). The [N/Fe] and [C/Fe] ratios for the giants analysed in this work show first dredge-up effects, but the [C/Fe] values are slightly high when we do not consider the uncertainties, as can be seen in Table 4. When ascending to the red giant branch, the abundance of ^{12}C is reduced as a consequence of the first dredge-up process and, the abundance of ^{14}N increases (Karakas & Lattanzio 2014), as it is clearly observed in all the giant stars analysed here.

Also, the abundance of lithium is expected to drop dramatically when stars evolve into RGB stage. Earlier and recent studies show that only 1–2 per cent of giants have log ϵ(Li) $\geq$ 1.50, which are the so-called lithium-rich giant stars – for more details about this topic see Holanda, Drake & Pereira (2020b), Holanda, Drake & Pereira (2020a), and the references therein. After NLTE corrections, we do not found significant enrichment of lithium in mean abundance for our sub-sample of four giants (1.08 dex), but the giants #29 and #233 present abundances near to the classical limit of 1.5 dex, which motivated us to discuss the abundance of lithium with additional attention.

It is well known in the literature that lithium overabundance may be associated with the high rotation in some giant stars and it is estimated that the coincidence of these aspects is around 50 per cent (Drake et al. 2002). According to Drake et al., #233 is not considered a rapid rotator (they consider rapid rotator stars only objects with v sin $i \geq 8.0\,\mathrm{km\,s^{-1}}$); however, it is an anomalous rotational velocity and the lithium preservation or production may be related to its atypical rotation. Moreover, #29 is a spectroscopic binary and is in the limit of rapid rotators (v sin $i = 10.0\,\mathrm{km\,s^{-1}}$) and also presents an anomalous lithium abundance [log $\epsilon(\mathrm{Li})_{\rm NLTE} = 1.39$]. In this discussion, we need to mention Casey et al. (2019) who suggest that tidal interactions between binaries are responsible for the lithium enrichment in giant stars.

For comparative proposes, we show in Fig. 10 (top panel) lithium abundances as a function of the projected rotational velocity for a sample of 67 red giants in 12 different open clusters studied by Delgado Mena et al. (2016). Despite the completeness of giants analysed by individuals open clusters of Delgado Mena et al.'s sample, we have constructed an analysis based on the mean lithium abundance and v sin i for each open cluster (bottom panel). In this respect, we can infer an increase of incidence of Li-enrichment with higher v sin i values. In bottom panel, NGC 6124 is the cluster with the highest mean v sin i value and is the one of the largest value of the lithium abundance: three of the four stars with determined abundance have showed log ϵ(Li) > 1.0, but #14 causes a significant decrease in the mean. This possible correlation it not new, for example, De Medeiros et al. (2000) carry out correlation coefficients for different mass intervals – between the mass intervals analysed by them, giants with masses of $3.5\,\mathrm{M}_\odot$ present a correlation coefficient value of 0.297 (poor correlation). Still, this is a questionable correlation since slow rotators are observed with different abundances of lithium, even among super Li-rich giants (Holanda et al. 2020a). This controversial point also is discussed by Magrini et al. (2021) who analysed a wide sample composed of main sequence, sub-giant, and giant stars in scope of the Gaia-ESO survey.

Recently, many studies have pointed out the importance of asteroseismology data to understand how and when lithium enrichment occurs after ascension to RGB (Singh et al. 2019; Martell et al. 2021; Yan et al. 2021; among others). There is a vast literature about models

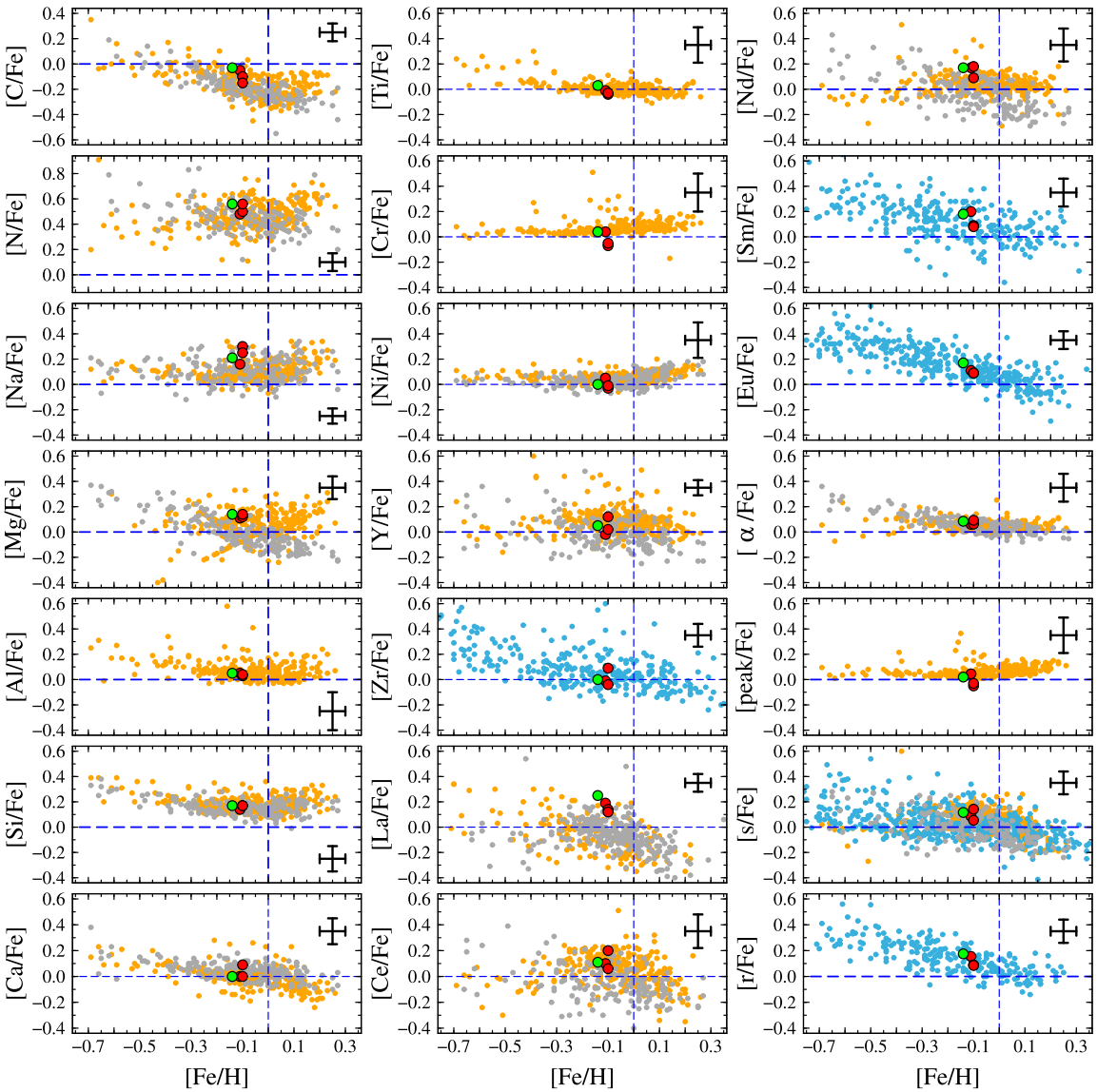

Figure 8. Abundance ratios [X/Fe] *versus* [Fe/H] for carbon to europium. [α/Fe], [peak/Fe], [s/Fe], [r/Fe] represent, respectively, the average for the α-elements (Si, Ca, Ti, Mg), iron-peak elements (Cr and Ni), the elements mostly created by the s-process (Y, Zr, La, Ce, and Nd), and the elements mostly created by the *r*-process (Sm and Eu). The red and green circles represent the giants analysed in this work, while the orange circles represent the abundances reported by Luck & Heiter (2007), the grey circles represent the abundances reported Mishenina et al. (2006, 2007) and the blue circles represent the abundances reported by Battistini & Bensby (2016). The blue dashed lines indicate solar values.

and alternative mechanisms candidates to explain the formation of Li-rich giants of low mass (log ϵ(Li) > 1.5), but it is out of context to our giant sample.

3.2.3 Na and Al elements and $^{12}C/^{13}C$ ratio

We provide abundances of Na I and Al I based on the cleanest and less blended lines present in our stellar spectra. In particular, the sodium abundance increases due to the first-dredge-up episode for a star that ascends to the red giant branch. However, a significant change is only remarkable for intermediate stellar masses ($M \geq 2.0\,M_{\odot}$) according to models for first-dredge-up (Karakas & Lattanzio 2014).

As is shown in Fig. 8, [Al/Fe] is in agreement and [Na/Fe] seems slightly enriched compared to the field stars and clump giants (Mishenina et al. 2006, 2007; Luck & Heiter 2007), but this comparison takes into account only the conditions based on LTE. After making corrections for NLTE conditions, stars have their sodium abundances reduced (in average by -0.06 dex). In addition, Fig. 11 presents the predictions for the abundance of $^{12}C/^{13}C$ isotopic ratio (top) and [Na/Fe] (bottom) and these results provide a new background about sodium and $^{12}C/^{13}C$ isotopic ratio that are traditional mixing tracers. This figure presents predictions for giants at the first dredge-up, using canonical and non-canonical models: thermohaline mixing from Charbonnel & Lagarde (2010) and Lagarde et al. (2012), thermohaline extra-mixing (Charbonnel & Lagarde 2010), and thermohaline and rotation-induced mixing (Lagarde et al. 2012); with all these models being relative to solar metallicity ($Z = 0.02$). The mean isotopic ratio $^{12}C/^{13}C$ and [Na/Fe] values, derived under LTE assumption (red circles) for the giants of NGC 6124 indicate a good agreement with the prediction

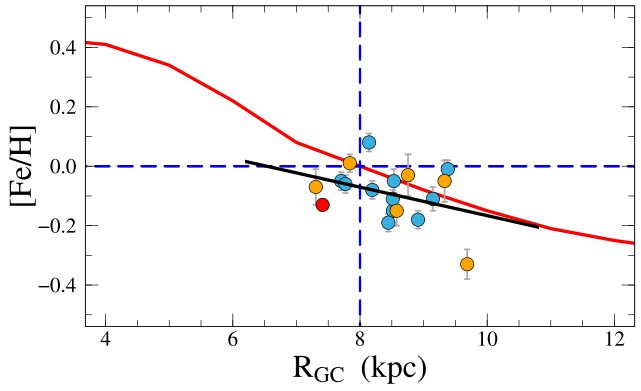

Figure 9. The average [Fe/H] versus Galactocentric distance with iron abundance gradients for open clusters – red solid curve is the model at present time from Magrini et al. (2009) and black line is our linear regression (slope = −0.048 ± 0.031). Blue dashed lines represent solar values for Galactocentric distance and [Fe/H]. The blue circles represent young open clusters (≤ 0.8 Gyr) with metallicities determined through high-resolution spectroscopy and analysed by Reddy, Lambert & Giridhar (2016). The orange circles are data obtained in our previous works (Santrich et al. 2013; Peña Suárez et al. 2018; da Silveira et al. 2018; Holanda et al. 2019; Martinez et al. 2020).

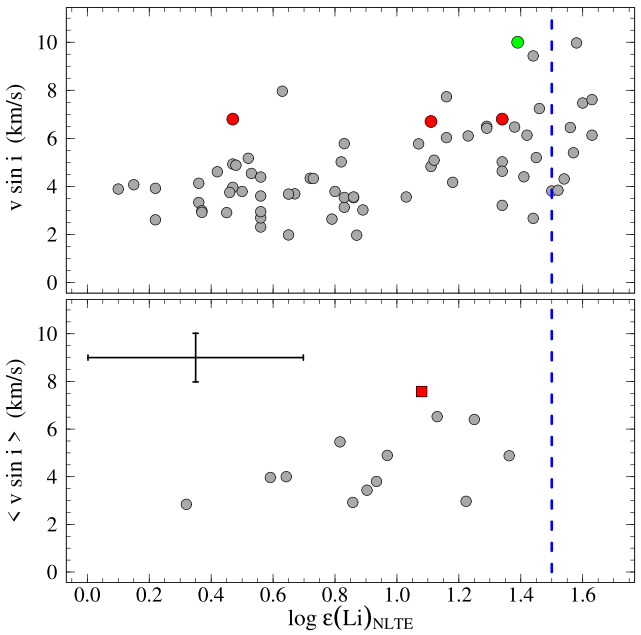

Figure 10. Lithium abundance versus projected rotational velocity v sin i. Our results are compared with a sample of open clusters analysed by Delgado Mena et al. (2016). In the top panel, we plotted individual values while in the bottom panel we present the mean rotational velocity for each open cluster. Horizontal blue dashed line represents the limit for normal and Li-rich giant stars (log ϵ(Li) = 1.5).

for thermohaline and the rotation-induced mixing from Lagarde et al. Nevertheless, according to the sodium abundance for a NLTE correction, [Na/Fe] NLTE (red triangle in bottom panel) and the turn-off mass value of our cluster, the abundance of this element is in good agreement with the predictions given by the first dredge-up.

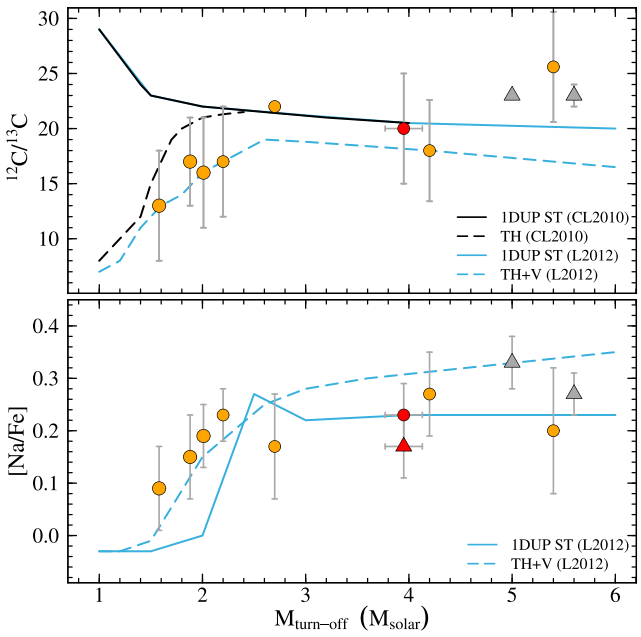

Figure 11. $^{12}C/^{13}C$ isotopic ratio (top) and [Na/Fe] (bottom) versus $M_{\rm turn\text{-}off}$ in giant stars of open clusters. In both panels, red symbols represent abundances for NGC 6124 when assuming LTE (circle) and NLTE (triangle) conditions; other symbols correspond to the mean $^{12}C/^{13}C$ isotopic ratio or [Na/Fe] for NGC 4609 and NGC 5316 (triangles; Drazdauskas et al. 2016) and open clusters previously studied by our group (orange circles; Santrich et al. 2013; da Silveira et al. 2018; Peña Suárez et al. 2018; Holanda et al. 2019; Martinez et al. 2020). Solid lines represent the predicted abundances of these elements for giants at the first dredge-up, using standard solar metallicity evolutionary models, from Charbonnel & Lagarde (Charbonnel & Lagarde, CL2010; black) and Lagarde et al. (2012, L2012; blue). Dashed lines indicate the prediction model for thermohaline extra-mixing and thermohaline and rotation-induced mixing from CL2010 (black) and L2012 (blue), respectively.

3.2.4 α-elements and iron-peak elements

The α-elements are produced on a time-scale of 10 Myr by massive stars, via type II supernovae (SN II). In Fig. 8, we compare our results with a sample of field stars. The abundance ratios [Ca/Fe], [Mg/Fe], and [Ti/Fe] have solar values and have basically the ratios in disc red clump giants and local disc field giants for the same metallicity (Mishenina et al. 2006, 2007; Luck & Heiter 2007). The [Si/Fe] ratio in NGC 6124 has a value of 0.16 dex with low scattering for the analysed giants here, but it is with good agreement with the considered samples of field stars.

The iron-peak elements, such as chromium and nickel, were also studied in this work. These two elements are produced mainly by Supernova Ia events, in a similar way to iron. For NGC 6124, we have found abundances similar to the solar values for both chemical species which is in a very good agreement with the giants analysed by Mishenina et al. (2006, 2007) and Luck & Heiter (2007).

3.2.5 Heavy elements

Elements with atomic number $Z > 30$ are called as 'heavy elements': these nucleus are formed by successive capture of neutrons by nucleus with $Z < 30$. The named 'slow' and 'rapid' neutron-capture processes are relative to time-scale of neutron-capture compared to β-decay (Burbidge et al. 1957).

Low- and intermediate-mass asymptotic giant branch stars are the main source for the formation of the elements created by slow neutron-capture process, s-process (Busso, Gallino & Wasserburg 1999). On other hand, r-elements have sources still widely discussed in the literature with the main origins remitting to production by neutrino-induced winds from SN II, merge between neutron stars and merger between neutron star and black hole (Woosley et al. 1994; Freiburghaus, Rosswog & Thielemann 1999; Surman et al. 2008). In this context, we measured abundances for some s-process elements produced in the first peak (Y and Zr) and second peak (La, Ce, and Nd) and also were determined the abundances of Sm and Eu elements – this last one a 'pure' r-process element, which is formed pre-dominantly due to an intense neutron flux (Bisterzo et al. 2016, 2017).

We calculated the mean abundance of the s-process elements[2] and compared the results for NGC 6124 with samples of giant and dwarf stars, as shown in Fig. 8. It can be seen that NGC 6124 presents a slight enrichment of s-process abundances compared to the sample of stars taken from the literature. In this context, D'Orazi et al. (2009) make the first report of a trend inversely proportional between barium abundances (a second peak element) and ages for a large sample of Galactic open clusters. Several other studies suggest that young open clusters are more enriched in the elements created by the s-process than the older open clusters (da Silveira et al. 2018; Magrini et al. 2018; Holanda et al. 2019; Martinez et al. 2020; among others).

In case of the elements pre-dominantly produced by the *r*-process, Sm and Eu, the abundances found in the giants of NGC 6124 cluster are in good agreement with the dwarf stars studied by Battistini & Bensby, when we compare stars of same metallicity.

4 CONCLUSIONS

The main findings based on the abundance analysis and projected rotational velocity employing high-resolution optical spectra on giants in open cluster NGC 6124 can be summarized as follows:

(i) The open cluster NGC 6124 has four rapid rotators ($v \sin i \geq 10.0\,\mathrm{km\,s^{-1}}$) and three moderate rotators $v \sin i \geq 6.0\,\mathrm{km\,s^{-1}}$, which is surprising since stellar evolution theory predicts low rotation for G–K red giant stars (de Medeiros, Da Rocha & Mayor 1996b; Carlberg et al. 2011). Among these stars, only two are classified as spectroscopic binaries while the others are single or wide binary stars. This high rotation velocity may be due to merger, tidal interactions, or swallowing of planets and/or brown dwarfs, as widely indicated in the literature.

(ii) We concluded that NGC 6124-33 is a cluster member. The robust membership analysis made in this work indicates a probability of 95 per cent for this object. NGC 6124-29 lies outside the characteristic overdensity that defines NGC 6124 in the parallax-magnitude diagram, having astrometric probability of only 39 per cent. This low astrometric probability of belong to cluster may due its nature, since this object was reported like spectroscopic binary (Mermilliod et al. 2008). However, abundances determined via equivalent width and spectral synthesis technique show that this star was born in the cluster, which is also supported by its proper motion and position in the colour–magnitude diagram.

(iii) In general, we note that abundances from NGC 6124 present a good agreement with abundances derived from field stars. However, it has been observed a possible correlation between the mean lithium abundance and the high mean for $v \sin i$ – this is an open issue, since exists considerable incidence of slow rotators with some enrichment in the data taken from the literature. In the context of giants belong to open clusters, our targets are notable by high rotational velocities and intermediate mean for Li abundances: the mean value drops because the low abundance observed in NGC 6124-14's atmosphere, a star with anomalous $v \sin i$ of $6.8\,\mathrm{km\,s^{-1}}$.

[2]defined as: [s/Fe] ≡ ([Y/Fe]+[Zr/Fe]+[La/Fe]+[Ce/Fe]+[Nd/Fe])/5

ACKNOWLEDGEMENTS

This study was financed in part by the agencies CNPq, FAPEMIG, FAPERJ, and CAPES (finance code 001). NAD acknowledges financial support by Russian Foundation for Basic Research (RFBR) according to the research projects 18-02-00554 and 18-52-06004. We also thank the referee, B. Twarog, for the valuable remarks that improved the paper. This research has made use of the SIMBAD and Vizier and data from the European Space Agency (ESA) mission *Gaia* (https://www.cosmos.esa.int/gaia), processed by the *Gaia* Data Processing and Analysis Consortium (DPAC; https://www.cosmos.esa.int/web/gaia/dpac/consortium). Funding for the DPAC has been provided by national institutions, in particular the institutions participating in the Gaia Multilateral Agreement.

Based on the observations made with the 2.2 m telescope at the European Southern Observatory (La Silla, Chile) under the agreement between Observatório Nacional and Max-Planck Institute für Astronomie.

DATA AVAILABILITY

The data underlying this article are publicly available (*Gaia* DR2 and EDR3) or are available in the article.

REFERENCES

Alonso A., Arribas S., Martínez-Roger C., 1999, A&AS, 140, 261
Alonso-Santiago J., Marco A., Negueruela I., Tabernero H. M., Castro N., McBride V. A., Rajoelimanana A. F., 2018, A&A, 616, A124
Alonso-Santiago J., Negueruela I., Marco A., Tabernero H. M., González-Fernández C., Castro N., 2019, A&A, 631, A124
Angelo M. S., Santos J. F. C., Corradi W. J. B., Maia F. F. S., 2019, A&A, 624, A8
Asplund M., Grevesse N., Sauval A. J., Scott P., 2009, ARA&A, 47, 481
Baratella M. et al., 2020, A&A, 634, A34
Battistini C., Bensby T., 2016, A&A, 586, A49
Baumgardt H., Dettbarn C., Wielen R., 2000, A&AS, 146, 251
Bauschlicher Charles W. J., Langhoff S. R., Taylor P. R., 1988, ApJ, 332, 531
Biazzo K., Randich S., Palla F., 2011, A&A, 525, A35
Bisterzo S. et al., 2016, J. Phys. Conf. Ser., 665, 012023
Bisterzo S., Travaglio C., Wiescher M., Käppeler F., Gallino R., 2017, ApJ, 835, 97
Böcek Topcu G., Afşar M., Sneden C., 2016, MNRAS, 463, 580
Burbidge E. M., Burbidge G. R., Fowler W. A., Hoyle F., 1957, Rev. Mod. Phys., 29, 547
Busso M., Gallino R., Wasserburg G. J., 1999, ARA&A, 37, 239
Cantat-Gaudin T. et al., 2018, A&A, 618, A93
Cardelli J. A., Clayton G. C., Mathis J. S., 1989, ApJ, 345, 245
Carlberg J. K., 2014, AJ, 147, 138
Carlberg J. K., Majewski S. R., Arras P., 2009, ApJ, 700, 832
Carlberg J. K., Majewski S. R., Patterson R. J., Bizyaev D., Smith V. V., Cunha K., 2011, ApJ, 732, 39
Casey A. R. et al., 2019, ApJ, 880, 125
Charbonnel C., Lagarde N., 2010, A&A, 522, A10
D'Orazi V., Magrini L., Randich S., Galli D., Busso M., Sestito P., 2009, ApJ, 693, L31

da Silveira M. D., Pereira C. B., Drake N. A., 2018, MNRAS, 476, 4907
Davis S. P., Phillips J. G., 1963, The Red System (A2[pi]-X2[Sigma]) of the CN Molecule. Univ. California Press, Berkeley
de Medeiros J. R., Da Rocha C., Mayor M., 1996b, A&A, 314, 499
De Medeiros J. R., do Nascimento J. D. J., Sankarankutty S., Costa J. M., Maia M. R. G., 2000, A&A, 363, 239
de Medeiros J. R., Melo C. H. F., Mayor M., 1996a, A&A, 309, 465
Deheuvels S., Ballot J., Beck P. G., Mosser B., Østensen R., García R. A., Goupil M. J., 2015, A&A, 580, A96
Delgado Mena E. et al., 2016, A&A, 587, A66
Dias W. S., Alessi B. S., Moitinho A., Lépine J. R. D., 2002, A&A, 389, 871
Drake N. A., de la Reza R., da Silva L., Lambert D. L., 2002, AJ, 123, 2703
Drake N. A., Pereira C. B., 2008, AJ, 135, 1070
Drazdauskas A., Tautvaišienė G., Smiljanic R., Bagdonas V., Chorniy Y., 2016, MNRAS, 462, 794
Fekel F. C., 1997, PASP, 109, 514
Fekel F. C., Balachandran S., 1993, ApJ, 403, 708
Ferreira F. A., Corradi W. J. B., Maia F. F. S., Angelo M. S., Santos J F C J., 2020, MNRAS, 496, 2021
Freiburghaus C., Rosswog S., Thielemann F. K., 1999, ApJ, 525, L121
Friel E. D., 1995, ARA&A, 33, 381
Gaia Collaboration et al., 2018, A&A, 616, A1
Gaia Collaboration et al., 2021, A&A, 649, A1
González Hernández J. I., Bonifacio P., 2009, A&A, 497, 497
Hatzidimitriou D. et al., 2019, A&A, 626, A90
Heiter U., Soubiran C., Netopil M., Paunzen E., 2014, A&A, 561, A93
Henden A. A., Levine S., Terrell D., Welch D. L., 2015, American Astronomical Society Meeting Abstracts #225. Vol. 225, 336.16
Hobbs L. M., Thorburn J. A., Rebull L. M., 1999, ApJ, 523, 797
Holanda N., Drake N.∼A., Pereira C.∼B., 2020a, MNRAS, 498, 77
Holanda N., Drake N. A., Pereira C. B., 2020b, AJ, 159, 9
Holanda N., Pereira C. B., Drake N. A., 2019, MNRAS, 482, 5275
Hou J. L., Prantzos N., Boissier S., 2000, A&A, 362, 921
Houk N., 1978, Michigan Catalogue of Two-dimensional Spectral Types for the HD Stars. University Microfilms International, Ann Arbor
Huber K., Herzberg G., 1979, Molecular Spectra and Molecular Structure. Van Nostrand Reinhold Company, New York
Karakas A. I., Lattanzio J. C., 2014, PASA, 31, e030
Kaufer A., Stahl O., Tubbesing S., Nørregaard P., Avila G., Francois P., Pasquini L., Pizzella A., 1999, Messenger, 95, 8
Kharchenko N. V., Piskunov A. E., Röser S., Schilbach E., Scholz R. D., 2005, A&A, 438, 1163
Koelbloed D., 1959, Bull. Astron. Inst. Netherlands, 14, 265
Kraft R. P., 1966, ApJ, 144, 1008
Kraft R. P., 1970, in Herbig G. H., Struve O., eds, Stellar Rotation. p. 385, Available at:https://ui.adsabs.harvard.edu/abs/1970saac.book..385K
Kurucz R., 1993, ATLAS9 Stellar Atmosphere Programs and 2 km/s grid. Kurucz CD-ROM No. 13. Cambridge, p. 13
Lada C. J., Lada E. A., 2003, ARA&A, 41, 57
Lagarde N., Decressin T., Charbonnel C., Eggenberger P., Ekström S., Palacios A., 2012, A&A, 543, A108
Lambert D. L., 1978, MNRAS, 182, 249
Lambert D. L., Heath J. E., Lemke M., Drake J., 1996, ApJS, 103, 183
Lawler J. E., Guzman A., Wood M. P., Sneden C., Cowan J. J., 2013, ApJS, 205, 11
Lawler J. E., Wickliffe M. E., den Hartog E. A., Sneden C., 2001, ApJ, 563, 1075
Lind K., Asplund M., Barklem P. S., 2009, A&A, 503, 541
Lind K., Asplund M., Barklem P. S., Belyaev A. K., 2011, A&A, 528, A103
Luck R. E., Heiter U., 2007, AJ, 133, 2464
Magrini L. et al., 2014, A&A, 563, A44
Magrini L. et al., 2017, A&A, 603, A2
Magrini L. et al., 2018, A&A, 617, A106
Magrini L. et al., 2021, AAP, 651, A84
Magrini L., Sestito P., Randich S., Galli D., 2009, A&A, 494, 95
Marigo P. et al., 2017, ApJ, 835, 77
Martell S. L. et al., 2021, MNRAS, 505, 5340
Martinez C. F., Holanda N., Pereira C. B., Drake N. A., 2020, MNRAS, 494, 1470
Massarotti A., Latham D. W., Stefanik R. P., Fogel J., 2008, AJ, 135, 209
Mermilliod J. C., Mayor M., Udry S., 2008, A&A, 485, 303
Mishenina T. V., Bienaymé O., Gorbaneva T. I., Charbonnel C., Soubiran C., Korotin S. A., Kovtyukh V. V., 2006, A&A, 456, 1109
Mishenina T.∼V., Gorbaneva T.∼I, Bienayme O, Soubiran C., Kovtyukh V.∼V., Orlova L.∼F., 2007, Astronomy Reports, 51, 382
Mucciarelli A., Caffau E., Freytag B., Ludwig H. G., Bonifacio P., 2008, A&A, 484, 841
Nesterov V. V., Kuzmin A. V., Ashimbaeva N. T., Volchkov A. A., Röser S., Bastian U., 1995, A&AS, 110, 367
Netopil M., Paunzen E., Heiter U., Soubiran C., 2016, A&A, 585, A150
O'Donnell J. E., 1994, ApJ, 422, 158
Pedreros M., 1987, AJ, 94, 1237
Peña Suárez V. J., Sales Silva J. V., Katime Santrich O. J., Drake N. A., Pereira C. B., 2018, ApJ, 854, 184
Peterson R. C., Tarbell T. D., Carney B. W., 1983, ApJ, 265, 972
Phillips J. G., Davis S. P., 1968, The Swan System of the C2 Molecule. The Spectrum of the HgH Molecule. Univ. California Press, Berkeley, CA
Piatti A. E., Clariá J. J., Bica E., Geisler D., Minniti D., 1998, AJ, 116, 801
Privitera G., Meynet G., Eggenberger P., Vidotto A. A., Villaver E., Bianda M., 2016, A&A, 593, A128
Reddy A. B. S., Lambert D. L., 2019, MNRAS, 485, 3623
Reddy A. B. S., Lambert D. L., Giridhar S., 2016, MNRAS, 463, 4366
Sales Silva J. V., Peña Suárez V. J., Katime Santrich O. J., Pereira C. B., Drake N. A., Roig F., 2014, AJ, 148, 83
Santrich O. J. K., Pereira C. B., Drake N. A., 2013, A&A, 554, A2
Siess L., Livio M., 1999, MNRAS, 308, 1133
Simon T., Drake S. A., 1989, ApJ, 346, 303
Singh R., Reddy B. E., Bharat Kumar Y., Antia H. M., 2019, ApJ, 878, L21
Smith V. V., Lambert D. L., Nissen P. E., 1998, ApJ, 506, 405
Sneden C. A., 1973, PhD thesis. Univ. Texas at Austin
Sneden C., Lambert D. L., 1982, ApJ, 259, 381
Spina L. et al., 2014, A&A, 568, A2
Spina L. et al., 2017, A&A, 601, A70
Sun W., de Grijs R., Deng L., Albrow M. D., 2019a, ApJ, 876, 113
Sun W., Li C., Deng L., de Grijs R., 2019b, ApJ, 883, 182
Surman R., McLaughlin G. C., Ruffert M., Janka H. T., Hix W. R., 2008, ApJ, 679, L117
The P. S., 1965, Contr. Bosscha Obs., 33, 1
Vergne M. M., Feinstein C., Martínez R., Orsatti A. M., Alvarez M. P., 2010, MNRAS, 403, 2041
Wood M. P., Lawler J. E., Sneden C., Cowan J. J., 2013, ApJS, 208, 27
Woosley S. E., Wilson J. R., Mathews G. J., Hoffman R. D., Meyer B. S., 1994, ApJ, 433, 229
Worley C. E., Douglass G. G., 1996, VizieR Online Data Catalog, p. I/237
Wyller A. A., 1966, ApJ, 143, 828
Yan H.-L. et al., 2021, Nature Astron., 5, 86

SUPPORTING INFORMATION

Supplementary data are available at *MNRAS* online.

Please note: Oxford University Press is not responsible for the content or functionality of any supporting materials supplied by the authors. Any queries (other than missing material) should be directed to the corresponding author for the article.

APPENDIX: EQUIVALENT WIDTHS MEASUREMENTS

See Tables A1 and A2.

Table A1. Observed iron and titanium lines. The column for each star shows the equivalent width in units of mÅ.

Element	λ (Å)	χ (eV)	log gf	Equivalent widths (mÅ) NGC 6124 - #			
				14	29	36	233
Fe I	5002.79	3.40	− 1.440	124	141	–	134
Fe I	5014.94	3.94	− 0.270	–	–	–	166
Fe I	5022.24	3.98	− 0.490	148	–	–	165
Fe I	5031.91	4.37	− 1.520	74	73	–	71
Fe I	5044.21	2.85	− 2.040	130	141	147	–
Fe I	5074.75	4.22	− 0.160	152	160	–	–
Fe I	5159.06	4.28	− 0.650	–	–	126	115
Fe I	5242.49	3.63	− 0.970	141	–	160	–
Fe I	5253.03	2.28	− 3.790	104	78	81	71
Fe I	5288.52	3.69	− 1.510	110	120	121	112
Fe I	5315.05	4.37	− 1.400	78	85	88	78
Fe I	5321.11	4.43	− 1.190	82	77	83	78
Fe I	5322.04	2.28	− 2.840	142	133	155	136
Fe I	5364.87	4.45	+0.230	–	159	–	–
Fe I	5373.71	4.47	− 0.710	96	99	111	104
Fe I	5389.48	4.42	− 0.250	–	–	143	135
Fe I	5417.03	4.42	− 1.530	72	69	74	68
Fe I	5441.34	4.31	− 1.580	79	69	73	67
Fe I	5445.04	4.39	+0.041	167	153	–	166
Fe I	5522.45	4.21	− 1.400	83	93	90	82
Fe I	5531.98	4.91	− 1.460	48	43	45	–
Fe I	5560.21	4.43	− 1.040	87	83	92	86
Fe I	5567.39	2.61	− 2.560	–	149	168	152
Fe I	5576.09	3.43	− 0.850	166	166	–	–
Fe I	5584.77	3.57	− 2.170	92	–	87	82
Fe I	5624.02	4.39	− 1.330	85	87	98	89
Fe I	5633.95	4.99	− 0.120	102	105	110	101
Fe I	5635.82	4.26	− 1.740	69	61	69	63
Fe I	5638.26	4.22	− 0.720	116	121	128	119
Fe I	5691.50	4.30	− 1.370	98	92	96	86
Fe I	5705.47	4.30	− 1.360	78	82	77	70
Fe I	5717.83	4.28	− 0.979	–	118	116	–
Fe I	5731.76	4.26	− 1.150	101	99	111	104
Fe I	5806.73	4.61	− 0.900	92	91	103	90
Fe I	5814.81	4.28	− 1.820	50	49	51	50
Fe I	5852.22	4.55	− 1.180	89	93	91	81
Fe I	5883.82	3.96	− 1.210	127	–	130	120
Fe I	5916.25	2.45	− 2.990	146	–	–	144
Fe I	5934.65	3.93	− 1.020	130	136	145	129
Fe I	6024.06	4.55	− 0.060	144	145	159	162
Fe I	6027.05	4.08	− 1.090	109	112	126	120
Fe I	6056.01	4.73	− 0.400	–	107	118	116
Fe I	6079.01	4.65	− 0.970	79	80	88	80
Fe I	6082.71	2.22	− 3.580	112	–	115	106
Fe I	6093.64	4.61	− 1.350	–	68	61	60
Fe I	6096.66	3.98	− 1.780	76	80	82	76
Fe I	6120.25	0.91	− 5.950	64	64	58	44
Fe I	6151.62	2.18	− 3.290	131	–	140	124
Fe I	6157.73	4.08	− 1.110	124	130	146	132
Fe I	6165.36	4.14	− 1.470	90	88	95	88
Fe I	6173.34	2.22	− 2.880	160	159	–	157
Fe I	6187.99	3.94	− 1.570	94	91	100	93
Fe I	6200.31	2.60	− 2.440	141	143	164	150
Fe I	6311.50	2.83	− 3.230	106	–	–	–
Fe I	6322.69	2.59	− 2.430	154	149	170	156
Fe I	6380.74	4.19	− 1.320	113	115	110	103
Fe I	6392.54	2.28	− 4.030	78	–	82	66
Fe I	6419.95	4.73	− 0.090	118	–	140	135
Fe I	6436.41	4.19	− 2.460	44	–	–	33
Fe I	6469.19	4.83	− 0.620	–	–	119	110
Fe I	6551.68	0.99	− 5.790	82	80	62	49
Fe I	6574.23	0.99	− 5.020	133	121	135	111
Fe I	6597.56	4.79	− 0.920	78	74	83	72
Fe I	6608.03	2.28	− 4.030	84	84	80	72
Fe I	6609.11	2.56	− 2.690	161	153	167	154
Fe I	6646.93	2.61	− 3.990	71	–	–	55
Fe I	6653.85	4.14	− 2.520	28	33	26	25
Fe I	6699.14	4.59	− 2.190	21	18	23	20
Fe I	6703.57	2.76	− 3.160	112	105	116	103
Fe I	6704.48	4.22	− 2.660	18	21	16	12
Fe I	6713.74	4.79	− 1.600	48	40	39	37
Fe I	6739.52	1.56	− 4.950	77	68	68	56
Fe I	6745.96	4.07	− 2.770	24	–	20	18
Fe I	6750.15	2.42	− 2.620	152	155	–	159
Fe I	6752.71	4.64	− 1.200	–	–	95	81
Fe I	6783.70	2.59	− 3.980	79	–	–	–
Fe I	6793.26	4.07	− 2.470	36	–	32	34
Fe I	6806.85	2.73	− 3.210	109	103	113	105
Fe I	6810.26	4.61	− 0.990	96	86	93	87
Fe I	6820.37	4.64	− 1.170	86	90	93	85
Fe I	6851.64	1.61	− 5.320	71	–	–	46
Fe I	6858.15	4.61	− 0.930	86	92	89	89
Fe I	7130.92	4.22	− 0.700	153	–	161	160
Fe I	7132.99	4.08	− 1.610	81	104	98	97
Fe II	4620.52	2.84	− 3.230	94	95	123	116
Fe II	4993.35	2.81	− 3.670	73	–	84	91
Fe II	5132.66	2.81	− 4.000	58	–	73	72
Fe II	5197.56	3.23	− 2.250	128	–	–	–
Fe II	5234.62	3.22	− 2.240	124	131	–	–
Fe II	5325.56	3.22	− 3.170	69	67	95	95
Fe II	5414.05	3.22	− 3.620	49	50	78	74
Fe II	5425.25	3.20	− 3.210	71	72	99	97
Fe II	5991.37	3.15	− 3.560	66	–	92	–
Fe II	6084.10	3.20	− 3.800	–	–	–	68
Fe II	6149.25	3.89	− 2.720	67	59	81	79
Fe II	6247.55	3.89	− 2.340	86	90	110	–
Fe II	6416.92	3.89	− 2.680	60	61	82	82
Fe II	6432.68	2.89	− 3.580	77	65	96	96
Ti I	4758.12	2.25	0.510	106	113	–	89
Ti I	4759.27	2.26	0.590	–	–	–	96
Ti I	4771.10	0.83	− 2.350	57	–	–	–
Ti I	4805.41	2.35	0.070	100	–	85	80
Ti I	4820.41	1.50	− 0.380	–	118	134	–
Ti I	4840.87	0.90	− 0.430	144	–	149	138
Ti I	4870.12	2.25	0.440	–	–	127	117
Ti I	4913.61	1.87	0.220	117	114	121	106
Ti I	4915.23	1.89	− 0.910	60	58	41	–
Ti I	4919.86	2.16	− 0.120	–	–	–	94
Ti I	4926.15	0.82	− 2.090	66	56	47	40
Ti I	5009.65	0.02	− 2.200	124	137	131	115
Ti I	5016.16	0.85	− 0.480	149	–	153	139
Ti I	5024.84	0.82	− 0.530	150	–	–	145
Ti I	5043.58	0.84	− 1.590	105	107	92	87
Ti I	5045.41	0.85	− 1.840	101	99	86	78
Ti I	5062.10	2.16	− 0.390	64	59	53	51
Ti I	5065.98	1.44	− 0.970	–	–	102	91
Ti I	5071.47	1.46	− 0.990	94	95	90	79
Ti I	5087.06	1.43	− 0.880	110	–	101	91
Ti I	5113.44	1.44	− 0.700	–	–	90	78

Table A1 – *continued*

Table A1 – *continued*

Element	λ (Å)	χ (eV)	log *gf*	Equivalent widths (mÅ) NGC 6124 - #			
				14	29	36	233
Ti I	5120.41	2.58	0.480	107	111	–	–
Ti I	5147.48	0.00	− 1.940	146	148	157	137
Ti I	5219.70	0.02	− 2.220	138	121	126	111
Ti I	5248.38	1.88	− 1.680	24	22	23	14
Ti I	5282.38	1.05	− 1.810	84	76	74	64
Ti I	5295.78	1.07	− 1.590	76	76	63	55
Ti I	5300.01	1.05	− 2.300	–	60	–	–
Ti I	5338.31	0.83	− 2.730	45	50	–	–
Ti I	5366.64	0.82	− 2.460	40	56	39	27
Ti I	5384.63	0.83	− 2.770	22	–	17	–
Ti I	5389.99	1.87	− 1.100	46	57	–	–
Ti I	5471.19	1.44	− 1.420	66	56	52	43
Ti I	5481.86	1.43	− 1.360	–	–	70	–
Ti I	5490.15	1.46	− 0.840	–	–	85	–
Ti I	5739.41	2.25	− 0.610	–	42	35	34
Ti I	5739.98	2.24	− 0.920	38	44	43	38
Ti I	5752.85	2.24	− 1.590	11	–	–	–
Ti I	5823.69	2.27	− 1.010	31	32	36	–
Ti I	5866.45	1.07	− 0.790	150	150	155	135
Ti I	5918.54	1.07	− 1.640	81	72	71	61
Ti I	5922.01	1.05	− 1.380	102	103	105	88
Ti I	5937.81	1.07	− 1.940	64	61	51	43
Ti I	5999.66	2.24	− 0.720	–	–	31	25
Ti I	6091.17	2.27	− 0.320	71	68	–	54
Ti I	6092.79	1.89	− 1.380	31	–	22	16
Ti I	6121.00	1.88	− 1.420	35	32	29	24
Ti I	6258.10	1.44	− 0.390	–	–	134	121
Ti I	6266.01	1.75	− 1.950	18	–	–	–
Ti I	6268.52	1.43	− 2.260	23	–	–	–
Ti I	6303.76	1.44	− 1.580	72	–	61	50
Ti I	6312.24	1.46	− 1.550	55	47	43	37
Ti I	6336.10	1.44	− 1.690	47	58	36	33
Ti I	6497.68	1.44	− 2.020	43	36	33	29
Ti I	6508.12	1.43	− 2.030	43	39	32	23
Ti I	6554.22	1.44	− 1.150	94	104	–	79
Ti I	6556.06	1.46	− 1.060	88	102	–	70
Ti II	4865.61	1.12	− 2.700	–	113	130	125
Ti II	4874.01	3.10	− 0.860	–	–	–	85
Ti II	5069.09	3.12	− 1.620	31	34	39	37
Ti II	5185.90	1.89	− 1.410	128	122	150	–
Ti II	5211.53	2.59	− 1.410	–	70	88	87
Ti II	5336.79	1.58	− 1.600	130	–	–	–
Ti II	5418.77	1.58	− 2.130	107	105	125	118
Ti II	6680.13	3.10	− 1.890	38	–	–	39

Table A2. Observed Na I to Sm II lines. The column for each star shows the equivalent width in units of mÅ.

Element	λ (Å)	χ (eV)	log *gf*	Equivalent Widths (mÅ) NGC 6124 - #			
				14	29	36	233
Na I	4751.82	2.10	− 2.095	–	–	–	35
Na I	5148.84	2.10	− 2.058	–	49	–	–
Na I	6154.22	2.10	− 1.560	85	–	95	85
Na I	6160.75	2.10	− 1.261	103	105	117	105
Mg I	4730.04	4.34	− 2.390	108	–	–	100
Mg I	5711.10	4.34	− 1.750	147	148	–	152
Mg I	8712.69	5.93	− 1.260	53	–	–	–
Mg I	8717.83	5.91	− 0.970	105	95	105	96
Mg I	8736.04	5.94	− 0.340	133	146	142	140
Al I	6696.03	3.14	− 1.481	76	–	–	–
Al I	6698.67	3.14	− 1.630	52	59	56	46
Al I	7835.32	4.04	− 0.580	73	79	–	72
Al I	7836.13	4.02	− 0.400	86	85	84	81
Al I	8772.88	4.02	− 0.250	119	100	116	107
Si I	5793.08	4.93	− 2.060	81	70	84	85
Si I	6125.03	5.61	− 1.540	46	48	61	55
Si I	6131.58	5.62	− 1.685	42	–	–	–
Si I	6145.02	5.61	− 1.430	52	57	63	60
Si I	6155.14	5.62	− 0.770	99	96	112	109
Si I	7760.64	6.20	− 1.280	22	26	32	31
Si I	7800.00	6.18	− 0.720	57	–	–	81
Si I	8728.01	6.18	− 0.360	–	–	–	93
Si I	8742.45	5.87	− 0.510	114	–	134	128
Ca I	5581.80	2.52	− 0.670	–	–	153	–
Ca I	5857.46	2.93	+0.110	161	–	–	–
Ca I	5867.57	2.93	− 1.610	52	54	50	55
Ca I	6161.30	2.52	− 1.270	122	129	128	118
Ca I	6166.44	2.52	− 1.140	122	118	129	123
Ca I	6169.04	2.52	− 0.800	145	146	–	149
Ca I	6169.56	2.53	− 0.480	161	–	–	169
Ca I	6449.82	2.52	− 0.500	–	–	–	157
Ca I	6455.60	2.51	− 1.290	116	114	119	112
Ca I	6471.66	2.51	− 0.690	150	147	–	146
Ca I	6499.65	2.52	− 0.810	145	–	–	152
Ca I	6798.47	2.71	− 2.520	24	–	20	19
Cr I	4790.34	2.54	− 1.480	60	59	51	44
Cr I	4836.87	3.10	− 1.090	56	–	54	49
Cr I	4936.34	3.11	− 0.250	–	–	86	77
Cr I	4953.71	3.12	− 1.480	–	–	20	–
Cr I	5013.31	2.71	− 0.770	100	–	–	–
Cr I	5067.72	2.71	− 1.070	90	94	88	77
Cr I	5144.66	2.71	− 1.371	68	62	67	55
Cr I	5192.00	3.39	− 0.400	–	–	68	–
Cr I	5200.21	3.38	− 0.580	72	–	–	–
Cr I	5238.96	2.71	− 1.270	–	55	44	40
Cr I	5241.45	2.71	− 1.921	–	–	18	13
Cr I	5272.01	3.45	− 0.420	–	–	50	–
Cr I	5287.20	3.44	− 0.870	37	43	39	35
Cr I	5304.18	3.46	− 0.670	51	50	–	31
Cr I	5318.81	3.44	− 0.670	43	50	43	–
Cr I	5344.79	3.45	− 0.990	28	–	17	–
Cr I	5628.62	3.42	− 0.740	41	–	38	–
Cr I	5712.75	3.01	− 1.030	72	68	–	45
Cr I	5719.81	3.01	− 1.580	–	24	26	24
Cr I	5787.04	3.01	− 1.551	40	34	–	30
Cr I	5788.39	3.01	− 1.491	31	37	33	20
Cr I	5844.59	3.01	− 1.772	31	–	–	–
Cr I	5884.43	3.01	− 1.860	16	–	–	–
Ni I	4519.98	1.68	− 3.080	–	–	–	108

Table A2 *– continued*

Element	λ (Å)	χ (eV)	log gf	Equivalent Widths (mÅ) NGC 6124 - #			
				14	29	36	233
Ni I	4866.27	3.54	− 0.220	–	120	–	131
Ni I	4953.21	3.74	− 0.580	105	96	119	108
Ni I	5003.75	1.68	− 3.070	–	–	–	91
Ni I	5010.94	3.63	− 0.979	89	81	99	91
Ni I	5157.98	3.61	− 1.510	–	–	50	42
Ni I	5388.34	1.94	− 3.510	77	74	74	68
Ni I	5435.86	1.99	− 2.580	116	112	135	–
Ni I	5578.73	1.68	− 2.830	127	127	–	–
Ni I	5587.87	1.94	− 2.390	–	–	143	–
Ni I	5748.36	1.68	− 3.240	–	–	107	98
Ni I	5847.01	1.68	− 3.460	94	–	98	–
Ni I	6007.31	1.68	− 3.400	–	–	88	82
Ni I	6108.12	1.68	− 2.600	151	–	–	154
Ni I	6128.98	1.68	− 3.429	102	103	110	104
Ni I	6176.82	4.09	− 0.260	–	93	104	101
Ni I	6177.25	1.83	− 3.460	68	65	68	60
Ni I	6204.61	4.09	− 1.080	–	63	60	55
Ni I	6223.99	4.11	− 0.910	60	62	60	59
Ni I	6327.60	1.68	− 3.170	122	121	130	–
Ni I	6378.26	4.15	− 0.821	75	–	81	71
Ni I	6532.87	1.94	− 3.350	76	–	–	68
Ni I	6586.32	1.95	− 2.780	118	110	126	115
Y II	5087.43	1.08	− 0.170	–	–	143	133
Y II	5200.41	0.99	− 0.570	–	–	–	127
Y II	5289.81	1.03	− 1.850	35	33	47	47
Y II	5402.78	1.84	− 0.440	60	57	74	76
Zr I	4772.30	0.62	− 0.060	49	49	35	37
Zr I	4815.63	0.60	− 0.270	–	–	22	–
Zr I	5385.13	0.52	− 0.640	–	25	20	–
Zr I	5680.91	0.54	− 0.860	–	–	–	13
Zr I	6127.46	0.15	− 1.060	42	38	30	22
Zr I	6134.57	0.00	− 1.280	35	30	27	21
Zr I	6143.18	0.07	− 1.100	46	43	37	30
La II	5303.53	0.32	− 1.350	46	–	49	47
La II	6320.43	0.17	− 1.520	53	46	50	41
La II	6348.48	0.32	− 1.410	45	–	–	–
La II	6774.33	0.12	− 1.709	42	40	53	49
Ce II	4418.79	0.86	+0.270	–	–	90	92
Ce II	4486.91	0.29	− 0.180	93	–	–	–
Ce II	4562.37	0.48	+0.210	91	90	–	115
Ce II	4628.16	0.52	+0.140	86	82	–	–
Ce II	5187.46	1.21	+0.170	47	47	59	59
Ce II	5274.24	1.04	+0.130	64	56	63	59
Ce II	5330.58	0.87	− 0.400	29	28	43	42
Ce II	5975.82	1.33	− 0.450	–	–	19	18
Ce II	6043.37	1.21	− 0.480	21	–	–	29
Nd II	4706.54	0.00	− 0.710	83	76	103	93
Nd II	4914.38	0.38	− 0.699	73	–	74	76
Nd II	4987.16	0.74	− 0.790	–	–	40	32
Nd II	5063.72	0.98	− 0.620	–	–	31	28
Nd II	5092.80	0.38	− 0.610	57	59	66	–
Nd II	5130.59	1.30	+0.450	–	–	66	–
Nd II	5234.19	0.55	− 0.510	–	61	–	81
Nd II	5293.16	0.82	+0.100	92	–	–	–
Nd II	5306.46	0.86	− 0.970	–	–	22	17
Nd II	5311.46	0.98	− 0.420	40	–	–	–
Nd II	5485.70	1.26	− 0.120	40	39	47	45
Nd II	5740.88	1.16	− 0.530	19	–	28	26
Nd II	5811.57	0.86	− 0.860	25	20	25	26
Sm II	4206.12	0.38	− 0.720	–	37	–	–
Sm II	4220.66	0.54	− 0.440	–	–	–	65

Table A2 *– continued*

Element	λ (Å)	χ (eV)	log gf	Equivalent Widths (mÅ) NGC 6124 - #			
				14	29	36	233
Sm II	4318.94	0.28	− 0.250	–	–	–	88
Sm II	4421.13	0.38	− 0.489	–	–	–	52
Sm II	4467.34	0.66	+0.150	–	–	–	66
Sm II	4478.65	0.66	− 0.360	–	47	60	–
Sm II	4499.48	0.25	− 0.870	–	–	44	41
Sm II	4523.91	0.43	− 0.390	–	–	72	–
Sm II	4566.20	0.33	− 0.590	55	–	–	54
Sm II	4642.23	0.38	− 0.460	67	59	67	59
Sm II	4676.90	0.04	− 0.870	68	56	64	55
Sm II	4704.40	0.00	− 0.860	–	59	82	74
Sm II	4791.60	0.10	− 1.440	–	26	30	28

This paper has been typeset from a TEX/LATEX file prepared by the author.